NASA/TM—2005-213421

Narrow Angle Wide Spectral Range Radiometer Design

FEANICS/REEFS Radiometer Design Report

William Camperchioli
Glenn Research Center, Cleveland, Ohio

January 2005

The NASA STI Program Office . . . in Profile

Since its founding, NASA has been dedicated to the advancement of aeronautics and space science. The NASA Scientific and Technical Information (STI) Program Office plays a key part in helping NASA maintain this important role.

The NASA STI Program Office is operated by Langley Research Center, the Lead Center for NASA's scientific and technical information. The NASA STI Program Office provides access to the NASA STI Database, the largest collection of aeronautical and space science STI in the world. The Program Office is also NASA's institutional mechanism for disseminating the results of its research and development activities. These results are published by NASA in the NASA STI Report Series, which includes the following report types:

- TECHNICAL PUBLICATION. Reports of completed research or a major significant phase of research that present the results of NASA programs and include extensive data or theoretical analysis. Includes compilations of significant scientific and technical data and information deemed to be of continuing reference value. NASA's counterpart of peer-reviewed formal professional papers but has less stringent limitations on manuscript length and extent of graphic presentations.

- TECHNICAL MEMORANDUM. Scientific and technical findings that are preliminary or of specialized interest, e.g., quick release reports, working papers, and bibliographies that contain minimal annotation. Does not contain extensive analysis.

- CONTRACTOR REPORT. Scientific and technical findings by NASA-sponsored contractors and grantees.

- CONFERENCE PUBLICATION. Collected papers from scientific and technical conferences, symposia, seminars, or other meetings sponsored or cosponsored by NASA.

- SPECIAL PUBLICATION. Scientific, technical, or historical information from NASA programs, projects, and missions, often concerned with subjects having substantial public interest.

- TECHNICAL TRANSLATION. English-language translations of foreign scientific and technical material pertinent to NASA's mission.

Specialized services that complement the STI Program Office's diverse offerings include creating custom thesauri, building customized databases, organizing and publishing research results . . . even providing videos.

For more information about the NASA STI Program Office, see the following:

- Access the NASA STI Program Home Page at ***http://www.sti.nasa.gov***

- E-mail your question via the Internet to help@sti.nasa.gov

- Fax your question to the NASA Access Help Desk at 301–621–0134

- Telephone the NASA Access Help Desk at 301–621–0390

- Write to:
  NASA Access Help Desk
  NASA Center for AeroSpace Information
  7121 Standard Drive
  Hanover, MD 21076

NASA/TM—2005-213421

Narrow Angle Wide Spectral Range Radiometer Design

FEANICS/REEFS Radiometer Design Report

William Camperchioli
Glenn Research Center, Cleveland, Ohio

National Aeronautics and
Space Administration

Glenn Research Center

January 2005

Available from

NASA Center for Aerospace Information
7121 Standard Drive
Hanover, MD 21076

National Technical Information Service
5285 Port Royal Road
Springfield, VA 22100

Available electronically at http://gltrs.grc.nasa.gov

Narrow Angle Wide Spectral Range Radiometer Design

FEANICS/REEFS Radiometer Design Report

William Camperchioli
National Aeronautics and Space Administration
Glenn Research Center
Cleveland, Ohio 44135

1. Background

A critical measurement for the Radiative Enhancement Effects on Flame Spread (REEFS) experiment is the net radiative flux emitted from the gasses and from the solid fuel bed. The scheme proposed to accomplish this measurement, as described in the REEFS Science Requirements Document (SRD), consists of a set of three narrow angle field of view (FOV) radiometers, one aligned to a hole in the fuel bed viewing from the top surface, one aligned to the same hole in the fuel bed viewing from the bottom surface and the third aligned to an area of the fuel bed adjacent to the hole viewing from the top surface.

In the desired configuration (SRD section 2.2.2) there are three sets of three radiometers per fuel sample. The top radiometers are fixed and are therefore common to all fuel samples. The bottom radiometers are mounted in the fuel holder assembly and each fuel sample has dedicated radiometers. The specifications listed in the SRD call for an accuracy of ±10 percent of the reading and an expected range of fluxes of 0.001 to 0.05 W/cm^2. The desired spectral range of the radiometers is 0.6 to 30 μm. Ground testing has shown the optimal hole size in the fuel to be 2.5 mm. The fuel is 12 mm thick. The geometry of the FEANICS/CIR hardware yields the following critical dimensions (table 1) for the radiometer design.

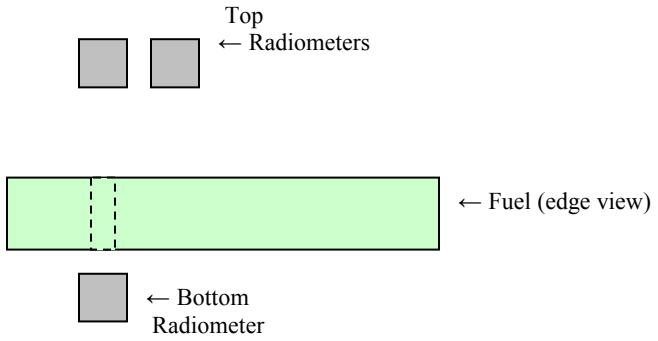

Figure 1.—REEFS radiometer configuration.

Table 1.—FEANICS/CIR hardware limiting dimensions

	Top Radiometer	Bottom Radiometer
Detector to fuel top surface distance(mm)	120	12
Maximum radiometer height (mm)	40	13

2. Design Choices

The spectral range requirement of 0.6 to 30 μm limits the choice of detectors to the thermopile type. A narrow angle field of view can be obtained using either a lens design or a pinhole arrangement "lensless" design. A lens design has the advantages of being able to focus and obtaining a higher sensitivity by utilizing a larger aperture compared to the lensless design. However, the index of refraction of lens materials varies with wavelength and 0.6 to 30 μm is a wide range. KRS-5 (Thallium Bromoiodide) is chosen as the optimal lens material since it transmits across the spectral range of 0.6 to 30 μm. If we assume the detector will be disc shaped with a diameter of 0.6 mm, and the desired FOV is 2.5 mm at a working distance of 120 mm we can calculate the required lens. The system magnification, m, equals

$$m = \frac{D_{detector}}{D_{FOV}} = \frac{0.6}{2.5} = 0.24 \tag{2–1}$$

The image distance (i), object distance (o) and magnification (m) are related by the equation

$$m = \frac{i}{o} \tag{2–2}$$

Therefore

$$i = m \times o = 0.24 \times 120 = 28.8 \text{ mm} \tag{2–3}$$

Using the Gaussian lens formula

$$\frac{1}{f} = \frac{1}{i} + \frac{1}{o} \tag{2–4}$$

$$f = \frac{1}{\left(\frac{1}{i} + \frac{1}{o}\right)} = \frac{1}{\left(\frac{1}{28.8} + \frac{1}{120}\right)} = 23.2 \text{ mm} \tag{2–5}$$

For a plano-convex lens, the radius of the convex surface (r), the focal length (f), and the index of refraction (n) are related by this reduction of the thin lens equation

$$r = f(n-1) \tag{2–6}$$

The index of refraction is a function of wavelength, for KRS-5, n varies from n = 2.60 at λ = 0.6 μm to n = 2.29 at λ = 30 μm. At n = 2.45, λ = 1.0 μm and

$$r = 23.2(2.45 - 1) = 33.64 \text{ mm} \tag{2–7}$$

Since the radius of curvature of the lens will be constant, the focal length will vary vs. wavelength due to the change in index of refraction. This spectrally dependent focal length will cause defocus and changes in the FOV.

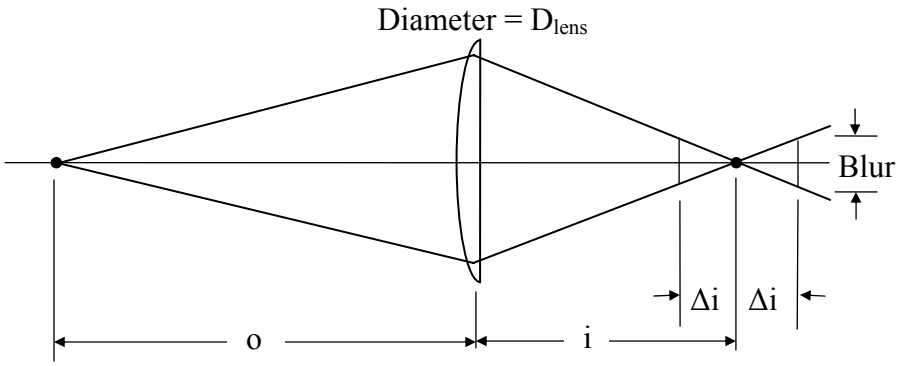

Figure 2.—Blur due to shift in image plane.

Referring to figure 2, for a thin lens optical system it can be seen that if the detector in the image plane is shifted along the optical axis by an amount Δi, then a point source in the object plane will no longer focus to a point in the image plane but will be a blur circle. The amount of blur can be calculated using similar triangles as

$$\frac{Blur}{\Delta i} = \frac{D_{lens}}{i} \tag{2–8}$$

$$\boxed{Blur = \frac{D_{lens}\Delta i}{i}} \tag{2–9}$$

where

$$i = \frac{1}{\left(\frac{1}{f} - \frac{1}{o}\right)} \tag{2–10}$$

$$f = \frac{r}{(n-1)} \tag{2–11}$$

$$\Delta i = \left| i - i_{\det ector} \right| \tag{2–12}$$

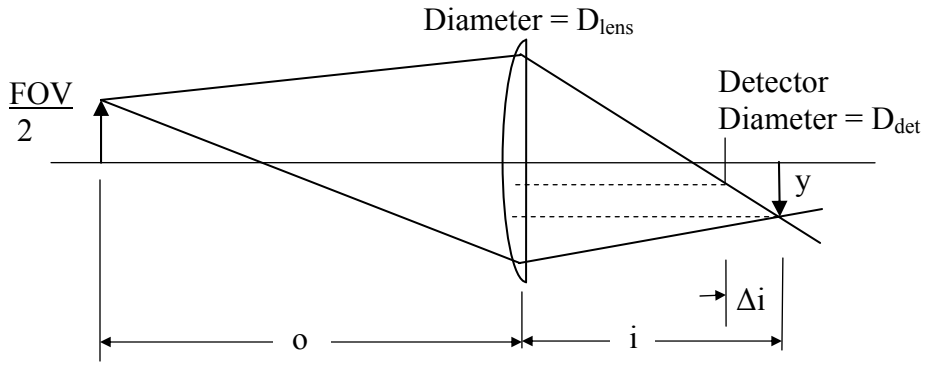

Figure 3.—FOV due to shift in image plane.

For the case where the detector is closer to lens than the image distance, *i*, the FOV in the object plane will be determined by the ray from the edge of the lens that intersects the edge of the detector. Referring to figure 3, we can again use similar triangles from the lens to the image plane to calculate

$$\frac{\left(\frac{D_{lens}}{2}+\frac{D_{\det}}{2}\right)}{i-\Delta i}=\frac{\left(\frac{D_{lens}}{2}+y\right)}{i} \tag{2–13}$$

$$2y=\left(\frac{i}{i-\Delta i}\right)\left(D_{lens}+D_{\det}\right)-D_{lens} \tag{2–14}$$

$$2y=\frac{iD_{lens}+iD_{\det}-iD_{lens}+\Delta iD_{lens}}{i-\Delta i}=\frac{iD_{\det}+\Delta iD_{lens}}{i-\Delta i} \tag{2–15}$$

By definition of magnification

$$m=\frac{y}{\left(\frac{FOV}{2}\right)} \tag{2–16}$$

$$2y=mFOV \tag{2–17}$$

For the radiometer, the detector will be at a fixed distance from the lens, $i_{\det}$, where

$$i_{\det}=i-\Delta i \tag{2–18}$$

The detector will have a designed magnification, m_{det}

$$m_{\text{det}} = \frac{i_{\text{det}}}{o} \tag{2–19}$$

Substituting equations (2–17) and (2–18) into equation (2–15) gives

$$mFOV = \frac{iD_{\text{det}} + \Delta iD_{lens}}{i_{\text{det}}} \tag{2–20}$$

$$FOV = \frac{iD_{\text{det}} + \Delta iD_{lens}}{mi_{\text{det}}} = \frac{iD_{\text{det}} + \Delta iD_{lens}}{\frac{i}{o}\left(i_{\text{det}}\right)} = \frac{D_{\text{det}} + \frac{\Delta iD_{lens}}{i}}{m_{\text{det}}} \tag{2–21}$$

$$\boxed{FOV = \frac{D_{\text{det}} + Blur}{m_{\text{det}}}} \tag{2–22}$$

If we design a lens based on $n = 2.45$, then $r = 33.64$ mm. This lens will have a focal length that varies from 21.0 mm at $n = 2.60$ to 26.1 mm at $n = 2.29$. Using an 8 mm diameter lens, this optical system will yield a spectrally dependent blur spot size and FOV as shown in table 2.

Based on these calculations, the Principal Investigator's concern over a spectrally dependent FOV and focus, and the success of the lensless radiometer described below, the decision was made to proceed with a lensless radiometer design.

Several earlier REEFS tests were conducted in the 2.2 second drop tower at NASA Glenn Research center utilizing the lensless radiometer shown in figure 4.

Table 2.—Spectral dependence of blur and FOV.

Dia Lens (mm)	λ (μm)	n	f (mm)	i (mm)	Δi (mm)	Blur (mm)	FOV (mm)
8	1.0	2.45	23.2	28.80	0.00	0.00	2.50
8	0.6	2.60	21.0	25.53	3.27	1.03	6.78
8	30.0	2.29	26.1	33.37	4.57	1.09	7.06

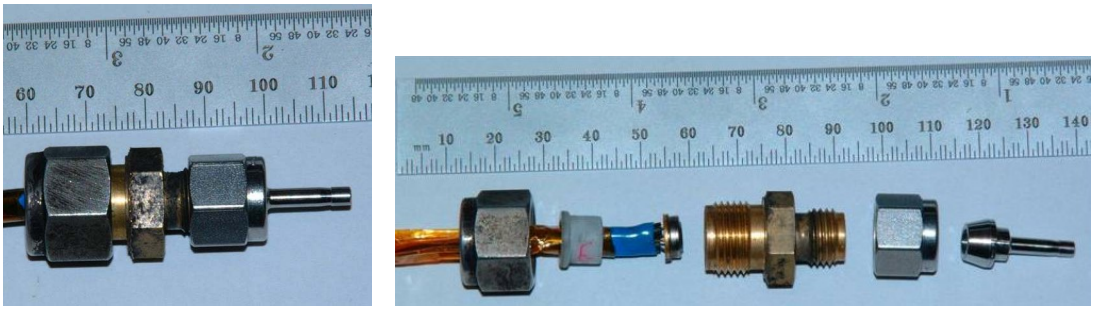

Figure 4.—REEFS 2.2 second drop tower radiometer.

The radiometer consists of a miniature thermopile detector (0.55 by 0.51 mm actual detector size), tube fittings and a 2 mm inside diameter tube to limit the FOV. The spacing from the detector to the front of the tube is 37.5 mm, and the distance from the front of the tube to the fuel surface was 75 mm. This radiometer was producing signals on the order of 200 to 300 mV with amplifier gain = 501.

3. Field of View

The FOV of a lensless radiometer will be a cone expanding from the front of the radiometer. The cone angle is determined by the size of the detector, the size of the aperture and the distance between the detector and the aperture. The FOV at the object plane will be a function of the size of the detector, the cone angle and the distance from the aperture to the object plane.

Referring to figure 5, it can be seen that there is not a sharp boundary of the FOV for a lensless radiometer. If both the detector and aperture are circular, parallel to each other and their centers are located on the same optical axis, then the FOV will be circular as well. The FOV will contain a central portion, called the umbra, in which every point will illuminate 100 percent of the detector. Detector response for a point source is uniform and maximum for every location in the umbra. For radii between umbra and penumbra the detector response due to a point source will decrease from maximum at $r = r_{umbra}$ to zero at $r = r_{penumbra}$. At radial distances > $r_{penumbra}$ the detector response due to a point source will be zero. The FOV will be as shown in figure 6.

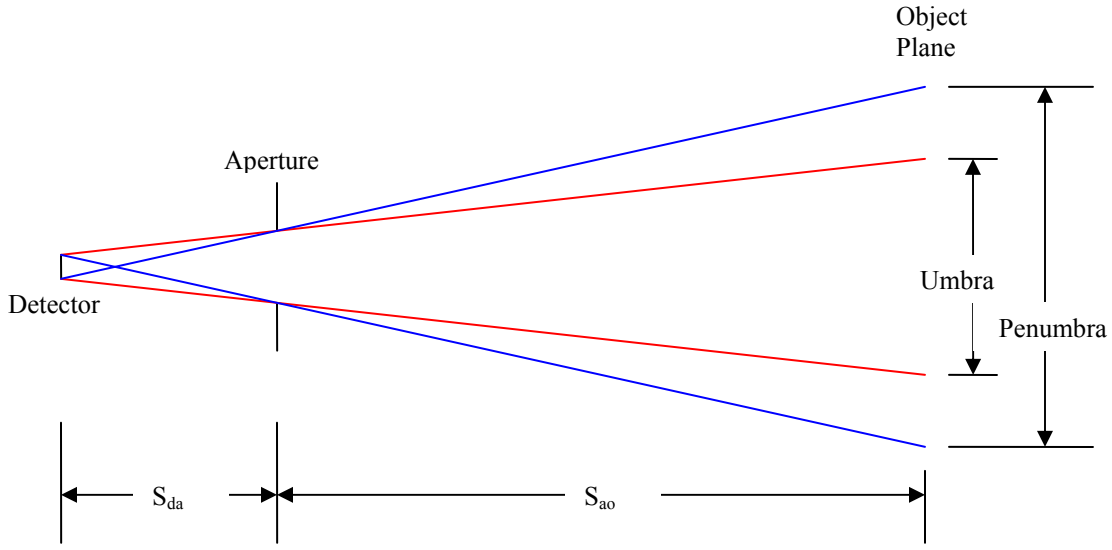

Figure 5.—Umbra and penumbra for a lensless radiometer.

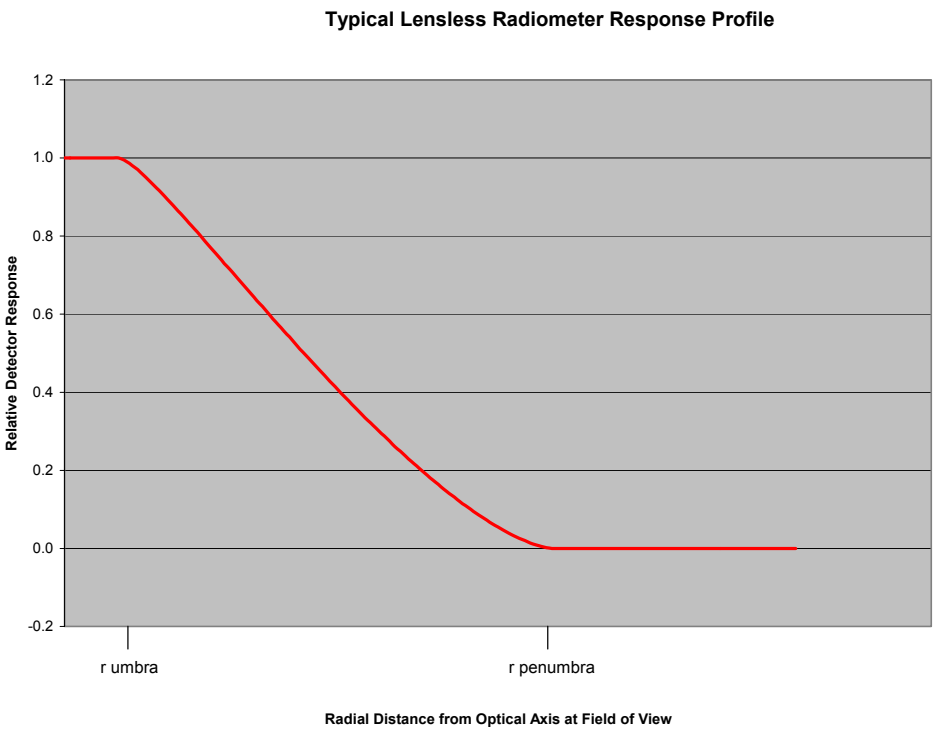

Figure 6(a).—Typical lensless radiometer response profile.

Figure 6(b).—Typical lensless radiometer response profile.

If we define

D_a diameter of the aperture
D_d diameter of the detector
D_u diameter of the umbra
D_p diameter of the penumbra
r_a radius of the aperture
r_d radius of the detector
r_u radius of the umbra
r_p radius of the penumbra

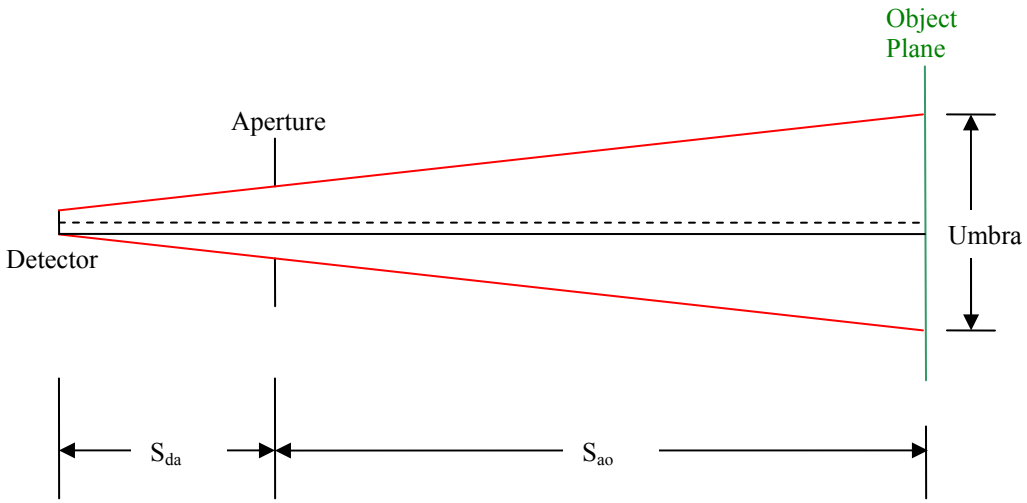

Figure 7.—Umbra for a lensless radiometer.

Referring to figure 7, using similar triangles, the radius of the umbra can be computed as

$$\frac{(r_u - r_d)}{(S_{da} + S_{ao})} = \frac{(r_a - r_d)}{S_{da}} \tag{3–1}$$

$$r_u = r_d + \frac{(S_{da} + S_{ao})}{S_{da}}(r_a - r_d) \tag{3–2}$$

$$r_u = \frac{r_d S_{da} + r_a(S_{da} + S_{ao}) - r_d S_{da} - r_d S_{ao}}{S_{da}} \tag{3–3}$$

$$r_u = \frac{r_a(S_{da} + S_{ao}) - r_d S_{ao}}{S_{da}} \tag{3–4}$$

The diameter of the umbra, which is the umbra FOV equals

$$D_u = \frac{D_a\left(S_{da} + S_{ao}\right) - D_d S_{ao}}{S_{da}} \tag{3–5}$$

Similarly, the diameter of the penumbra, which is the penumbra FOV equals

$$D_p = \frac{D_a\left(S_{da} + S_{ao}\right) + D_d S_{ao}}{S_{da}} \tag{3–6}$$

The REEFS radiometer used in the 2.2 second drop tower described above (fig. 4) has the following dimensions:

D_d = 0.6 mm (equivalent area of a square 0.55 × 0.51 mm detector)
D_a = 2 mm
S_{da} = 37.5 mm
S_{ao} = 75 mm

This yields the following:

Umbra = 4.8 mm
Penumbra = 7.2 mm

The FOV of this radiometer is not actually circular due to the rectangular shape of the detector. Although the above calculations are not exact they are adequate for comparison purposes.

The detector chosen for the REEFS radiometers is a silicon based thermopile detector with an active area of 0.6 by 0.6 mm. In order to provide a circular FOV for the radiometer, the detector is ordered with a 0.6 mm circular aperture placed directly on the active surface. Table 3 shows the calculated FOV for the current design.

The calculation for the top radiometer actually yields an umbra with a negative sign. This is a result of the pinhole diameter, D_a, being smaller than the detector diameter, D_d. The negative sign corresponds to the crossing of the umbra traces as shown in figure 8 below (compare to fig. 5 where the umbra traces do not cross). Practically speaking, the relationship between umbra and penumbra in both cases are similar.

Table 3.—FEANICS/REEFS radiometer calculated FOV.

Radiometer	Dd Detector Diameter (mm)	Da Pinhole Diameter (mm)	Sda Detector to Pinhole (mm)	Sdo Pinhole to Fuel Surface (mm)	Umbra at Fuel Surface (mm)	Penumbra at Fuel Surface (mm)
Top	0.6	0.3	30	120	-0.90	3.90
Bottom	0.6	0.6	8.5	12	0.60	2.29

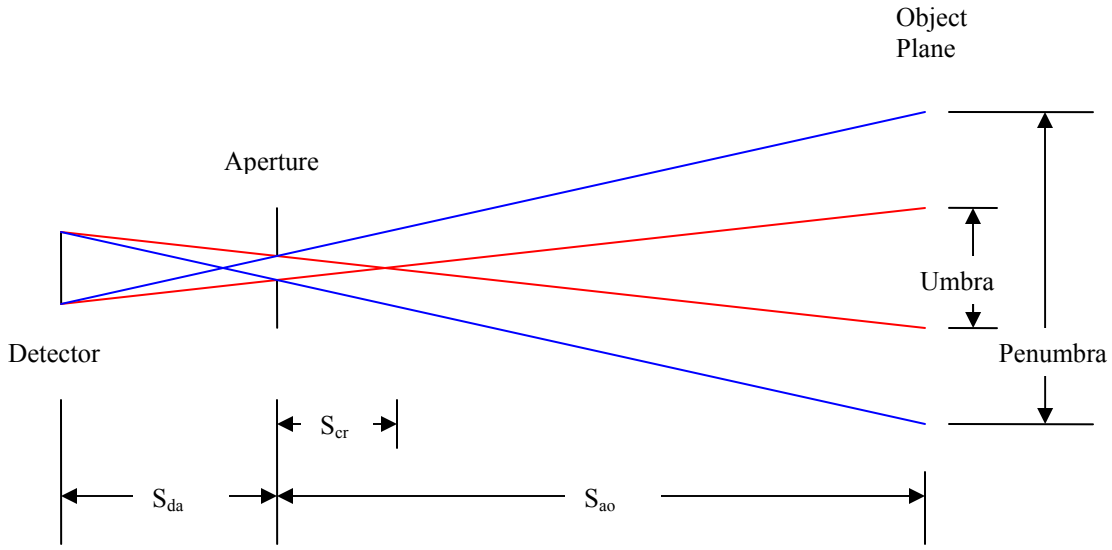

Figure 8.—Umbra and penumbra for a lensless radiometer with the aperture diameter smaller than the detector diameter.

Referring to figure 8, at a given distance from the aperture, S_{ao}, all points within the umbra will radiate onto an equal area of the detector. For distances closer to the aperture than the point where the umbra traces cross, S_{cr}, a point source within the umbra traces will radiate 100 percent of the detector area. For $S_{ao} > S_{cr}$, a point source cannot radiate 100 percent of the detector, but any point source at a given S_{ao} within the umbra will radiate the same percentage of the detector area. This can easily be proven as follows: any point source at a given S_{ao} will radiate to the aperture, which has a constant area. The aperture area can then be projected to the detector plane which is at a distance S_{da} from the aperture. Since S_{ao}, S_{da} and the aperture diameter are constant for all point sources it can be shown using similar triangles that every point will radiate to an equal area in the detector plane. Points inside the umbra will impinge upon the entire detector. Points outside the umbra but inside the penumbra will impinge upon a portion of the detector. Points outside of the penumbra will not impinge upon the detector. Therefore the FOV profile will be as shown in figure 6.

4. Radiometer Response

The response or sensitivity of a lensless radiometer will primarily be a function of the responsivity of the detector and the throughput of the system. The responsivity of the detector is determined by the physical design of the detector and its encapsulating gas. The trade off in choosing an encapsulating gas is sensitivity vs. response time. A gas that increases sensitivity will yield a slower response time.

The throughput of a lensless radiometer is dependent upon the geometry of the system and the transmission of the medium. For a uniform extended source the distance between the source and the aperture is unimportant as long as the source overfills the field of view of the radiometer. The radiation transfer from a source can be computed using an imaginary disc at the aperture as the source since this disc will subtend the same solid angle as that of the source at any distance in space. The radiation transfer for the lensless radiometer consisting of an ideal circular detector and a circular aperture normal and concentric to the axis joining them and a uniform extended source is

$$\Phi = \frac{2L\left(\pi r_d r_a\right)^2}{r_a^2 + r_d^2 + S_{da}^2 + \sqrt{\left(r_a^2 + r_d^2 + S_{da}^2\right)^2 - 4r_a^2 r_d^2}} \quad \text{(ref. 1, p. 24.17)} \qquad (4\text{–}1)$$

where

Φ radiant power on the detector (W)
L radiance of the source (W/sr m^2)

If optics with transmission, τ, are placed between the source and detector the radiation transfer becomes

$$\Phi = \frac{2\tau L\left(\pi r_d r_a\right)^2}{r_a^2 + r_d^2 + S_{da}^2 + \sqrt{\left(r_a^2 + r_d^2 + S_{da}^2\right)^2 - 4r_a^2 r_d^2}} \tag{4–2}$$

If the throughput, *T*, is defined as

$$\Phi = TL \tag{4–3}$$

Then

$$T = \frac{2\tau\left(\pi r_d r_a\right)^2}{r_a^2 + r_d^2 + S_{da}^2 + \sqrt{\left(r_a^2 + r_d^2 + S_{da}^2\right)^2 - 4r_a^2 r_d^2}} \tag{4–4}$$

where
τ transmission between the source and detector
r_a radius of the aperture
r_d radius of the detector
S_{da} distance between the detector and the aperture

If

$$(r_d^2 + r_a^2 + S_{da}^2) >> 4r_a^2 r_d^2 \text{ and } S_{da}^2 >> (r_d^2 + r_a^2)$$

Then the throughput reduces to

$$T = \frac{\tau A_d A_a}{S_{da}^2} \tag{4–5}$$

where
A_d the detector area
A_a the aperture area

The radiant power on the detector due to the source is

$$\boxed{\Phi = \frac{\tau A_d A_a L}{S_{da}^2} \quad \text{Watts}} \tag{4–6}$$

5. Radiometric Calculations

A basic thermopile detector consists of several thermocouple junctions attached to a black disc. As radiation impinges on the black disc its temperature will raise which in turn will cause the thermocouple voltage to increase. If properly calibrated the detector voltage output can provide an indication of source radiance. Referring to figure 9, what is of interest is the net radiant heat exchange between the detector and the source viewed through the aperture. From equation (4–6) the radiant power on the detector due to the source is

$$\Phi_s = \frac{\tau A_d A_a L_s}{S_{da}^2} \quad \text{Watts} \tag{5–1}$$

where
Φ_s radiant power on the detector due to the source (W)
L_s radiance of the source (W/sr m^2)

Following the same derivation method used in section 4 (Radiometer Response), it can be shown that the radiant power transferred from the detector to the source is:

$$\Phi_d = \frac{\tau A_d A_a L_d}{S_{da}^2} \quad \text{Watts} \tag{5–2}$$

where
Φ_d radiant power at the source due to the detector (W)
L_d radiance of the detector (W/sr m^2)

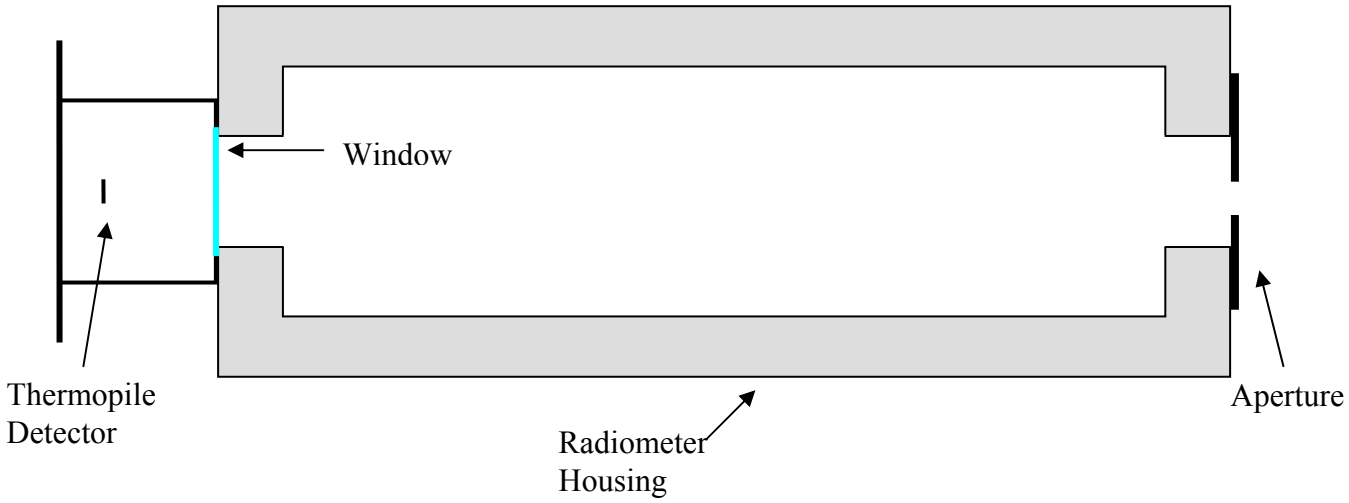

Figure 9.—Basic lensless radiometer.

But the radiant power leaving the detector directed toward the source, Φ'_d has not passed through the window and thus has no transmission loss. Therefore

$$\Phi'_d = \frac{A_d A_a L_d}{S_{da}^2} \quad \text{Watts} \tag{5–3}$$

For the window

$$\tau + \alpha + \rho = 1 \tag{5–4}$$

where
τ window transmission
α window absorption
ρ window reflection

if we assume that $\alpha \sim 0$, then

$$\tau + \rho = 1 \tag{5–5}$$

$$\rho = 1 - \tau \tag{5–6}$$

Since the window reflections are specular, and the cone angle between the detector and the source is small, we can make the simplifying assumption that all radiant power emanating from the detector toward the source, reflected by the window is directed back to the detector. This power, Φ_{dr}, will be

$$\Phi_{dr} = \frac{\rho A_d A_a L_d}{S_{da}^2} \quad Watts \tag{5–7}$$

$$\Phi_{dr} = \frac{(1-\tau) A_d A_a L_d}{S_{da}^2} \quad Watts \tag{5–8}$$

Therefore the net radiant heat exchange from the source to the detector is

$$\Phi = \Phi_s - \Phi'_d + \Phi_{dr} \tag{5–9}$$

$$\Phi = \frac{\tau A_d A_a L_s}{S_{da}^2} - \frac{A_d A_a L_d}{S_{da}^2} + \frac{(1-\tau) A_d A_a L_d}{S_{da}^2} \tag{5–10}$$

$$\Phi = \frac{\tau A_d A_a (L_s - L_d)}{S_{da}^2} \tag{5–11}$$

The radiance, L, can be calculated by the Stefan-Boltzmann law

$$L = \frac{\varepsilon \sigma T^4}{\pi} \quad \left(\frac{W}{cm^2 sr} \right) \tag{5–12}$$

where
ε emissivity
σ Stefan-Boltzmann constant = 5.6703E-12 W/cm^{2}K^4
T temperature in K

The responsivity, $\Re$, of a thermopile detector is defined as the detector output voltage, *Vo*, divided by the power on the detector, Φ.

$$\Re = \frac{V_o}{\Phi} \quad \left(\frac{V}{W}\right) \tag{5–13}$$

Substituting

$$\Phi = \frac{\tau A_d A_a \left(L_s - L_d\right)}{S_{da}^2} \tag{5–14}$$

Yields

$$V_o = \frac{\Re \tau A_d A_a \left(L_s - L_d\right)}{S_{da}^2} \quad (V) \tag{5–15}$$

$$L_s = \frac{V_o S_{da}^2}{\Re \tau A_d A_a} + L_d \quad \left(\frac{W}{cm^2 sr}\right) \tag{5–16}$$

$$L_s = \frac{V_o S_{da}^2}{\Re \tau A_d A_a} + \frac{\varepsilon \sigma}{\pi} T_d^4 \quad \left(\frac{W}{cm^2 sr}\right) \tag{5–17}$$

For the detector, ε ~ 1

$$\boxed{L_s = \frac{V_o S_{da}^2}{\Re \tau A_d A_a} + \frac{\sigma}{\pi} T_d^4 \quad \left(\frac{W}{cm^2 sr}\right)} \tag{5–18}$$

For a uniform extended source the exitance, *M*, is equal to:

$$M = \pi L \quad \left(\frac{W}{cm^2}\right) \text{ (ref. 6, p. 49)} \tag{5–19}$$

$$\boxed{M_s = \frac{\pi V_o S_{da}^2}{\Re \tau A_d A_a} + \sigma T_d^4 \quad \left(\frac{W}{cm^2}\right)} \tag{5–20}$$

If what is of interest is the change in radiance due to flame or hot gases passing the radiometer field of view, then the equations will be modified.

If we define
L_i the initial, non flame, background radiance
L_f radiance when flame front is in FOV

Then
ΔL radiance due to flame only

$$\Delta L = L_f - L_i \tag{5–21}$$

$$\Delta L = \left(\frac{V_{of} S_{da}^2}{\Re \tau A_d A_a} + \frac{\sigma}{\pi} T_d^4 \right) - \left(\frac{V_{oi} S_{da}^2}{\Re \tau A_d A_a} + \frac{\sigma}{\pi} T_d^4 \right) \quad \left(\frac{W}{cm^2 sr} \right) \tag{5–22}$$

where
V_{oi} initial radiometer output voltage, non flame, background radiance
V_{of} radiometer output voltage when flame front is in FOV

If the detector temperature is constant then

$$\Delta L = \left(V_{of} - V_{oi} \right) \frac{S_{da}^2}{\Re \tau A_d A_a} \qquad \left(\frac{W}{cm^2 sr} \right) \tag{5–23}$$

$$\Delta M = \left(V_{of} - V_{oi} \right) \frac{\pi S_{da}^2}{\Re \tau A_d A_a} \qquad \left(\frac{W}{cm^2} \right) \tag{5–24}$$

It is interesting to note that for the change in radiance or exitance, ΔL or ΔM, the assumption that all of the radiant power emanating from the detector, reflected by the window, is directed back to the detector is irrelevant. This assumption only effects the scaling of the $\frac{\sigma}{\pi} T_d^4$ term (Eq. (5–22)), which is cancelled in the subtraction.

6. Temperature Effects

If a measurement of the absolute radiance or exitance is desired, it can be seen from equations (5–18) and (5–20) that the detector temperature must be known. In addition a thermopile detector radiometer is very sensitive to temperature variations which will result in measurement errors. These temperature variations will induce errors into the system through different avenues.

6.1 Errors Due to Changes in Detector Temperature

Referring to equations (5–18) and (5–22) it is apparent that if the detector temperature, *Td*, changes between the initial background radiance reading and the flame radiance reading then there will be an error in the measured radiance of

$$\Delta L(error) = \frac{\sigma}{\pi} \left(T_{df}^4 - T_{di}^4 \right) \tag{6–1}$$

For this error it is not critical that the detector temperature be held at an absolute temperature, but that it remains at a constant temperature during the duration of the test.

Another error introduced into equation (5–18) due to changes in detector temperature is the responsivity, *R*, temperature coefficient. The responsivity changes, non-linearly with temperature. For this error the absolute temperature of the detector is critical and should be the same as the radiometer calibration temperature. A typical value for the temperature coefficient of responsivity for a thermopile detector is –0.01 percent/°C, based on a linear fit from 20 to 40 °C. This is a relatively small error over a fairly large temperature range.

The detector noise is also a function of detector temperature. The Johnson (thermal) noise of the detector is given by

$$V_n = \sqrt{4kTRB} \quad Vrms \text{ (ref. 2, p. 153)} \tag{6–2}$$

where

k Boltzmann's constant, 1.38065×10^{-23} J/K
T detector temperature in Kelvin
R detector resistance in ohms
B detector equivalent noise bandwidth

The change in thermal noise between the detector operating at room temperature, T_1 = 296 K, and the detector maximum temperature, T_2 = 273 + 85 = 358 K, is

$$\frac{V_{n2}}{V_{n1}} = \frac{\sqrt{4kT_2RB}}{\sqrt{4kT_1RB}} = \sqrt{\frac{T_2}{T_1}} = \sqrt{\frac{358}{296}} = 1.10 \tag{6–3}$$

Elevating the detector temperature to its maximum will increase the detector noise voltage by 10 percent over the room temperature noise voltage. As shown in table 6, the detector noise voltage is only a small fraction of the overall noise of the radiometer system. A 10 percent increase in the detector noise is insignificant compared to the total radiometer noise therefore the detector operating temperature is not limited by detector thermal noise concerns.

6.2 Errors Due to Changes in the Cold Junction

A thermopile detector consists of a blackened receiving surface which will rise in temperature upon absorbing incident radiation. The thermal circuit is shown in figure 10.

$$\Delta T = T - To = \alpha\Phi R_T \text{ (DC Case) (ref. 2, p. 165)} \tag{6–4}$$

α absorptance of the detector
Φ incident power on the detector
R_T thermal resistance between the detector and the heat sink

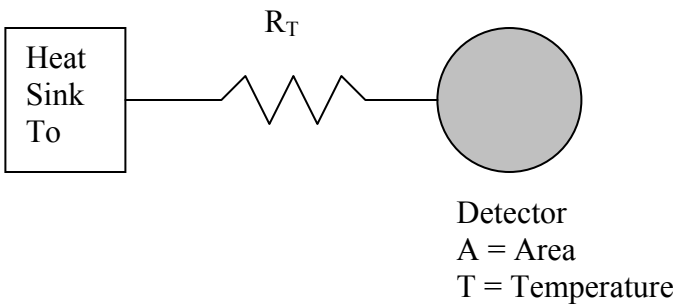

Figure 10.—Thermopile detector thermal circuit.

The detector voltage is measured with a thermopile with cold junction referenced to the heat sink. The Seebeck voltage, *S*, defines the thermopile output voltage.

$$S = \frac{\Delta V}{\Delta T} \tag{6–5}$$

The responsivity is

$$\Re = \frac{\Delta V}{\Phi} \tag{6–6}$$

$$\Delta V = \Re\Phi \tag{6–7}$$

$$S = \frac{\Re\Phi}{\alpha\Phi R_T} = \frac{\Re}{\alpha R_T} \tag{6–8}$$

The theoretical limit for R_T is

$$R_T = \frac{1}{4\alpha\sigma A T^3} \text{ (ref. 2, p. 165)} \tag{6–9}$$

Therefore

$$S = 4\Re\sigma A T^3 \quad (V/°K) \tag{6–10}$$

Ideally the radiometer will output a voltage, ΔV, proportional to a change in detector temperature, ΔT, due to incident radiation on the detector receiving area. If the cold junction, *To*, changes temperature independent of the detector temperature, *T*, from an outside source, then an output voltage will be produced

$$\Delta V = S\Delta T \quad (Volts) \tag{6–11}$$

This output voltage will be indiscernible from the output voltage due to the incident radiation.

For the chosen thermopile detector

$\Re$ = 101 V/W
A = 0.0036 cm^2
T = 296 K

Substituting in to equation (6–10) gives

$$S = 214 \quad \frac{\mu V}{K} \text{ (maximum)}$$

REEFS ground tests utilizing this detector in the current top radiometer design typically output 5 μV full scale. The detector and cold junction are designed to be closely coupled to eliminate these effects, but in cases of very low signal extra care needs to be given to reduce these effects. In the case of the chosen thermopile detector, the cold junction is located near the rear of the detector housing. Air currents or other heat or cold sources near the rear of the detector must be eliminated to prevent cold junction effects from saturating the detector signal.

6.3 Radiometer Housing Temperature Effects

Figure 11 shows a typical lensless radiometer with some critical dimensions defined. The aperture, detector and window are all assumed to be circular, normal and concentric to the axis joining them.

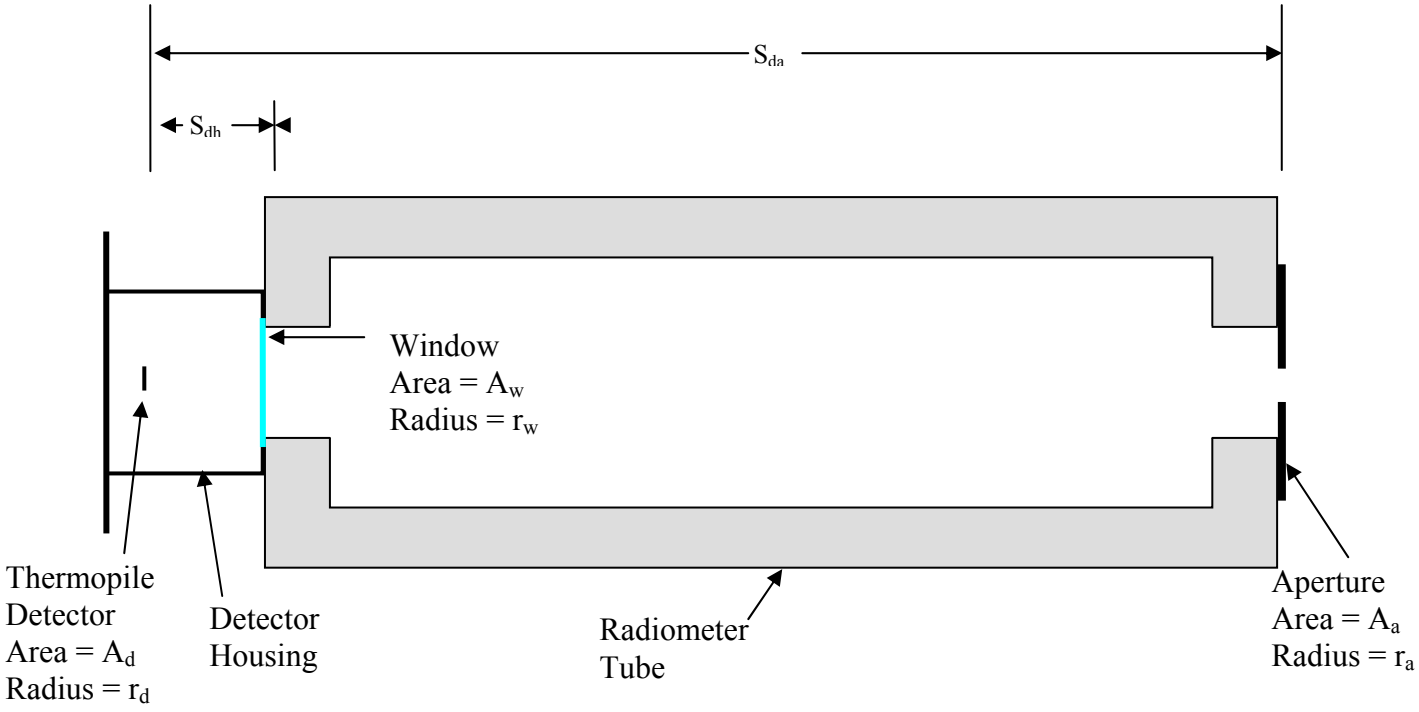

Figure 11.—Basic lensless radiometer.

For any two black body objects in space, the net radiant heat exchange from object 1 to object 2, Φ_{1-2}, can be defined as

$$\Phi_{1-2} = A_1 F_{1-2} \sigma\left(T_1^4 - T_2^4\right) \quad \text{(Watts)} \text{ (ref. 3, p. 32)} \tag{6–12}$$

where
A_1 area of object 1
σ Stefan-Boltzmann constant
F_{1-2} configuration factor from object 1 to object 2

The configuration factor is essentially the fraction of energy leaving object 1 that is intercepted by object 2.

Siegel and Howell (ref. 4) provide a detailed discussion on the calculation of configuration factors as well as an extensive catalog of their results. As published by Siegel and Howell (ref. 4, p. 845), for the case of two discs, normal and concentric to the axis joining them, the configuration factor is

$$R_1 = \frac{r_1}{h} \tag{6–13}$$

$$R_2 = \frac{r_2}{h} \tag{6–14}$$

$$X = 1 + \frac{1 + R_2^2}{R_1^2} \tag{6–15}$$

$$F_{1-2} = \frac{1}{2}\left[X - \sqrt{X^2 - 4\left(\frac{R_2}{R_1}\right)^2}\right] \tag{6–16}$$

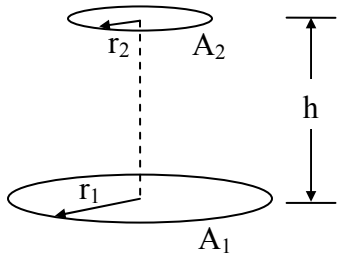

Figure 12.—Configuration factor for two discs.

For the case of the radiometer shown in figure 11, the configuration factor from the aperture to the detector, F_{1-2}, is

$$R_1 = \frac{r_a}{S_{da}} \tag{6–17}$$

$$R_2 = \frac{r_d}{S_{da}} \tag{6–18}$$

$$X = 1 + \frac{\left(1 + \left(\frac{r_d}{S_{da}}\right)^2\right)}{\left(\frac{r_a}{S_{da}}\right)^2} = 1 + \frac{S_{da}^2 + r_d^2}{r_a^2} = \frac{S_{da}^2 + r_a^2 + r_d^2}{r_a^2} \tag{6–19}$$

$$F_{a-d} = \frac{1}{2}\left[\frac{S_{da}^2 + r_a^2 + r_d^2}{r_a^2} - \sqrt{\left(\frac{S_{da}^2 + r_a^2 + r_d^2}{r_a^2}\right)^2 - 4\left(\frac{\left(\frac{r_d}{S_{da}}\right)^2}{\left(\frac{r_a}{S_{da}}\right)^2}\right)}\right] \tag{6–20}$$

$$F_{a-d} = \frac{1}{2r_a^2}\left[S_{da}^2 + r_a^2 + r_d^2 - \sqrt{\left(S_{da}^2 + r_a^2 + r_d^2\right)^2 - 4r_a^2 r_d^2}\right] \tag{6–21}$$

If we define

$$C = S_{da}^2 + r_a^2 + r_d^2 \tag{6–22}$$

then

$$F_{a-d} = \frac{1}{2r_a^2}\left[C - \sqrt{C^2 - 4r_a^2 r_d^2}\right] \tag{6–23}$$

$$F_{a-d} = \frac{\left(C - \sqrt{C^2 - 4r_a^2 r_d^2}\right)}{\left(2r_a^2\right)} \bullet \frac{\left(C + \sqrt{C^2 - 4r_a^2 r_d^2}\right)}{\left(C + \sqrt{C^2 - 4r_a^2 r_d^2}\right)} = \frac{C^2 - \left(C^2 - 4r_a^2 r_d^2\right)}{2r_a^2\left(C + \sqrt{C^2 - 4r_a^2 r_d^2}\right)} \tag{6–24}$$

$$F_{a-d} = \frac{\left(C^2 - C^2\right) + 4r_a^2 r_d^2}{2r_a^2\left(C + \sqrt{C^2 - 4r_a^2 r_d^2}\right)} = \frac{4r_a^2 r_d^2}{2r_a^2\left(C + \sqrt{C^2 - 4r_a^2 r_d^2}\right)} = \frac{2r_d^2}{C + \sqrt{C^2 - 4r_a^2 r_d^2}} \tag{6–25}$$

Substituting *C* into equation (6–25) gives

$$F_{a-d} = \frac{2r_d^2}{S_{da}^2 + r_a^2 + r_d^2 + \sqrt{\left(S_{da}^2 + r_a^2 + r_d^2\right)^2 - 4r_a^2 r_d^2}} \tag{6–26}$$

The radiant power transferred from the aperture to the detector, assuming the source at the aperture behaves as a black body, is:

$$\Phi_{a-d} = A_a F_{a-d} \sigma (T_1^4 - T_2^4) \tag{6–27}$$

$$\Phi_{a-d} = \frac{2r_d^2 A_a \sigma (T_a^4 - T_d^4)}{S_{da}^2 + r_a^2 + r_d^2 + \sqrt{\left(S_{da}^2 + r_a^2 + r_d^2\right)^2 - 4r_a^2 r_d^2}} \tag{6–28}$$

$$\Phi_{a-d} = \frac{2\pi\left(r_a r_d\right)^2 \sigma\left(T_a^4 - T_d^4\right)}{S_{da}^2 + r_a^2 + r_d^2 + \sqrt{\left(S_{da}^2 + r_a^2 + r_d^2\right)^2 - 4r_a^2 r_d^2}} \tag{6–29}$$

The Stefan-Boltzmann law states that the exitance, M, of a black body is equal to

$$M = \sigma T^4 \quad \text{(ref. 6, p. 11)} \tag{6–30}$$

For a Lambertian source we can substitute equation (5–19) to calculate the radiance, L

$$L = \frac{\sigma T^4}{\pi} \tag{6–31}$$

Substituting equation (6–31) into equation (6–29) gives

$$\Phi_{a-d} = \frac{2(\pi r_a r_d)^2 (L_a - L_d)}{S_{da}^2 + r_a^2 + r_d^2 + \sqrt{(S_{da}^2 + r_a^2 + r_d^2)^2 - 4r_a^2 r_d^2}} \tag{6–32}$$

For the case of the ideal detector, $L_d = 0$

$$\boxed{\Phi_{a-d} = \frac{2L_a (\pi r_a r_d)^2}{S_{da}^2 + r_a^2 + r_d^2 + \sqrt{(S_{da}^2 + r_a^2 + r_d^2)^2 - 4r_a^2 r_d^2}}} \tag{6–33}$$

It is interesting to note that equation (6–33) is the same as equation (4–1) presented in section 4 (Radiometer Reponses). The fact that the same result was obtained provides confidence in the derivation presented above.

For the case where the distance between the detector and aperture is much greater than the radius of the aperture and much greater than the radius of the detector, then $(r_d^2 + r_a^2 + S_{da}^2) >> 4r_a^2 r_d^2$ and $S_{da}^2 >> (r_d^2 + r_a^2)$, and equation (6–32) reduces to

$$\boxed{\Phi_{a-d} = \frac{(\pi r_a r_d)^2 (L_a - L_d)}{S_{da}^2} = \frac{A_a A_d (L_a - L_d)}{S_{da}^2}} \tag{6–34}$$

It is interesting to note that equation (6–34) is the same as equation (5–11) presented in section 5 (Radiometric Calculations), with $\tau = 1$. The fact that the same result was obtained provides confidence in the derivations presented above and in section 5.

The radiant heat exchange between the source viewed through the aperture and the detector is the measurement of interest. Referring to figure 11, the detector actually sees radiation from the entire 2π steradian, hemisphere field of view. If we divide the detector field of view into regions, the net radiant heat exchange from each region can then be computed to determine the contribution from each part. The detector net radiant heat exchange can be divided into three components; 1. The net radiant heat exchange between the detector housing and the detector (Φ_{h-d}), 2. The net radiant heat exchange between the radiometer tube and the detector (Φ_{t-d}), 3. The net radiant heat exchange between the aperture opening and the detector (Φ_{a-d}). Even though the last component is that which is of interest, the following discussion reveals that the radiometer is very sensitive to changes in temperature of the radiometer tube and of the detector housing and such can easily swamp the measure of the phenomenon of interest.

The total net radiant heat transfer to the detector will be the sum of the three components.

$$\Phi_{net} = \Phi_{h-d} + \Phi_{t-d} + \Phi_{a-d} \tag{6–35}$$

If we put an imaginary disc at the window surface we can then define the configuration factor from the detector to the window surface as F_{d-w} and the configuration factor from the detector to the housing as F_{d-h}. Since all of the energy leaving the detector reaches either the window surface or the housing

$$1 = F_{d-w} + F_{d-h} \tag{6–36}$$

and

$$F_{d-h} = 1 - F_{d-w} \tag{6–37}$$

The law of view factor reciprocity (ref. 3, p. 539) states

$$A_1 F_{1-2} = A_2 F_{2-1} \tag{6–38}$$

Therefore the configuration factor from the housing to the detector is

$$F_{h-d} = \frac{A_d}{A_h}\left(F_{d-h}\right) = \frac{A_d}{A_h}\left(1 - F_{d-w}\right) \tag{6–39}$$

Since the detector housing is aluminum it has an emissivity, $\varepsilon < 1$, and cannot be approximated as a black body. The radiative heat transfer between two gray bodies is

$$\Phi_{1-2} = \frac{\sigma\left(T_1^4 - T_2^4\right)}{\frac{1-\varepsilon_1}{\varepsilon_1 A_1} + \frac{1}{A_1 F_{1-2}} + \frac{1-\varepsilon_2}{\varepsilon_2 A_2}} \text{ (ref. 3, p. 550)} \tag{6–40}$$

Therefore

$$\Phi_{h-d} = \frac{\sigma\left(T_h^4 - T_d^4\right)}{\frac{1-\varepsilon_h}{\varepsilon_h A_h} + \frac{1}{A_h F_{h-d}} + \frac{1-\varepsilon_d}{\varepsilon_d A_d}} \tag{6–41}$$

The detector has an emissivity close to 1, so if we set $\varepsilon_d = 1$, and substitute equation (6–39)

$$\boxed{\Phi_{h-d} = \frac{\sigma\left(T_h^4 - T_d^4\right)}{\frac{1-\varepsilon_h}{\varepsilon_h A_h} + \frac{1}{A_d\left(1 - F_{d-w}\right)}}} \tag{6–42}$$

Assuming the source viewed through the aperture behaves as a black body, the net radiant heat exchange from the aperture to the detector is

$$\Phi_{a-d} = A_a F_{a-d} \sigma\left(T_a^4 - T_d^4\right) = A_d F_{d-a} \sigma\left(T_a^4 - T_d^4\right) \tag{6–43}$$

From equation (6–36)

$$1 = F_{d-w} + F_{d-h} \tag{6–44}$$

$$1 = F_{d-w} + F_{d-h} - F_{d-a} + F_{d-a} = F_{d-h} + \left(F_{d-w} - F_{d-a}\right) + F_{d-a} \tag{6–45}$$

Therefore the configuration factor from the detector to the radiometer tube is

$$F_{d-t} = F_{d-w} - F_{d-a} \tag{6–46}$$

and

$$F_{t-d} = \frac{A_d}{A_t} F_{d-t} = \frac{A_d}{A_t}\left(F_{d-w} - F_{d-a}\right) \tag{6–47}$$

The radiometer tube is blackened to absorb reflections, so assuming the emissivity of the tube = 1, the net radiant heat exchange from the radiometer tube to the detector will be

$$\Phi_{t-d} = A_t F_{t-d} \sigma\left(T_t^4 - T_d^4\right) \tag{6–48}$$

$$\Phi_{t-d} = A_t \left(\frac{A_d}{A_t}\left(F_{d-w} - F_{d-a}\right) \right) \sigma\left(T_t^4 - T_d^4\right) \tag{6–49}$$

$$\Phi_{t-d} = A_d \left(F_{d-w} - F_{d-a}\right) \sigma\left(T_t^4 - T_d^4\right) \tag{6–50}$$

The total net radiant heat exchange to the detector is

$$\Phi_{net} = \Phi_{h-d} + \Phi_{t-d} + \Phi_{a-d} \tag{6–51}$$

$$\Phi_{net} = \underbrace{\left\{ \frac{\sigma\left(T_h^4 - T_d^4\right)}{\frac{1-\varepsilon_h}{\varepsilon_h A_h} + \frac{1}{A_d\left(1 - F_{d-w}\right)}} \right\}}_{\text{Detector Housing}} + \underbrace{\left\{A_d \left(F_{d-w} - F_{d-a}\right) \sigma\left(T_w^4 - T_d^4\right)\right\}}_{\text{Radiometer Tube}} + \underbrace{\left\{A_d F_{d-a} \sigma\left(T_a^4 - T_d^4\right)\right\}}_{\text{Aperture}} \quad (W) \tag{6–52}$$

The three terms in brackets in the above equation (6–52) each represent the net effect of the corresponding component on the detector. The first term is the fraction of the radiant power heat exchange due to the detector housing, the second term is the fraction of the radiant power heat exchange due to the radiometer tube, and the third term is the fraction of the radiant power heat exchange due to the signal through the aperture (the source).

The third term is the desired measurement. The first two terms are considered error terms due to differences in the radiometer housing temperature and the detector temperature. Notice that if any component and the detector are at the same temperature, that term goes to zero.

From equation (6–26), the configuration factor for two discs, orthogonal and concentric to the axis joining them is

$$F_{a-d} = \frac{2r_d^2}{S_{da}^2 + r_a^2 + r_d^2 + \sqrt{\left(S_{da}^2 + r_a^2 + r_d^2\right)^2 - 4r_a^2 r_d^2}} \tag{6–53}$$

Therefore

$$F_{d-w} = \frac{2r_w^2}{S_{dh}^2 + r_d^2 + r_w^2 + \sqrt{\left(S_{dh}^2 + r_d^2 + r_w^2\right)^2 - 4r_d^2 r_w^2}} \tag{6–54}$$

$$F_{d-a} = \frac{2r_a^2}{S_{da}^2 + r_d^2 + r_a^2 + \sqrt{\left(S_{da}^2 + r_d^2 + r_a^2\right)^2 - 4r_d^2 r_a^2}} \tag{6–55}$$

The current FEANICS/REEFS top radiometer design has the following dimensions

S_{da} = 30 mm
S_{dh} = 4.75 mm
r_d = 0.3 mm
r_w = 1.0 mm
r_a = 0.15 mm
A_d = 0.283 mm^2
A_h = 174 mm^2
ε_h = 0.095 (source Siegel and Howell)

Solving equation (6–52) using these numbers gives

$$\Phi = 1.5\times10^{-14}\left(T_h^4 - T_d^4\right) + 6.8\times10^{-16}\left(T_w^4 - T_d^4\right) + 4.0\times10^{-19}\left(T_a^4 - T_d^4\right) \quad (Watts) \tag{6–56}$$

Using this result the radiometer response due to each component relative to the desired measurement (aperture response) can be computed.

$$\frac{\Phi_{\text{detector housing}}}{\Phi_{aperture}} = \frac{1.5\times10^{-14}}{4.0\times10^{-19}} = 37{,}500 \tag{6–57}$$

$$\frac{\Phi_{radiometer\ tube}}{\Phi_{aperture}} = \frac{6.8\times10^{-16}}{4.0\times10^{-19}} = 1{,}700 \tag{6–58}$$

This means that the radiometer is 37,500 times more sensitive to temperature changes in the detector housing than to temperature changes in the source being measured and 1,700 times more sensitive to temperature changes in the radiometer tube than in the source being measured.

Another way to look at the temperature effect is to assume the detector described above has a responsivity of 69 V/W and the source emits radiation equivalent to a black body at 650 K. If the detector, detector housing and radiometer tube are all at the same temperature, $T = 296$ K, then the radiometer output signal will be

$$V_o = \Re\Phi = 69 \times 4.0 \times 10^{-19}\left(650^4 - 296^4\right) = 4.7\mu V \tag{6–59}$$

The equivalent change in the radiometer tube temperature to produce the same signal is

$$V_o = \Re\Phi = 69 \times 6.8 \times 10^{-16}\left(T^4 - 296^4\right) = 4.7\mu V \tag{6–60}$$

$$T = \left(\frac{4.7 \times 10^{-6}}{69 \times 6.8 \times 10^{-16}} + 296^4\right)^{\frac{1}{4}} = 296.96K \tag{6–61}$$

$$\boxed{\Delta T = T - T_d = 296.96 - 296 = 0.96 \cong 1K} \tag{6–62}$$

Similarly the equivalent change in the detector housing temperature to produce the same signal is

$$V_o = \Re\phi = 69 \times 1.5 \times 10^{-14}\left(T^4 - 296^4\right) = 4.7\mu V \tag{6–63}$$

$$T = \left(\frac{4.7 \times 10^{-6}}{69 \times 1.5 \times 10^{-14}} + 296^4\right)^{\frac{1}{4}} = 296.04K \tag{6–64}$$

$$\boxed{\Delta T = T - T_d = 296.04 - 296 = 0.04K} \tag{6–65}$$

This shows how sensitive the radiometer is to temperature variations. The above exercise breaks down the radiometer system into three components, the detector housing, the radiometer tube and the aperture opening. If desired, the system could be broken down into more components using the method as above. In practice each component will not be at one temperature and the detector at another temperature, there will more likely be a temperature gradient from one component to the next, but the above derivation gives an "order of magnitude" indication of the temperature effects of the radiometer.

Controlled cooling of the detector in a radiometer is a common method of increasing the signal output and stabilizing the detector temperature drift. As shown in equation (6–58) the FEANICS/REEFS radiometer is 1700 times more sensitive to changes in the radiometer tube temperature than to changes in the source temperature viewed through the aperture. A typical detector cooler will cool the detector and detector housing. For the FEANICS/REEFS radiometer the radiometer tube is also the holder for the entire radiometer assembly, and has a lot of mass compared to the detector and its housing. Since the radiometer is so sensitive to the radiometer tube temperature, the cooling system would have to cool the detector, the detector housing and the entire radiometer tube to a uniform temperature. Cooling only the detector and its housing, or having a difference of only a couple of degrees C between the detector and the

radiometer tube would saturate the output signal. A cooling system to meet these specifications is not trivial and would pose several engineering challenges.

Let's suppose that the challenges were met and an ideal cooling system for this radiometer was designed and built. This ideal cooling system would cool the detector, detector housing and radiometer tube all to 0 K, with no temperature variations. Since the detector housing and radiometer tube terms would be zero, the net radiant heat exchange to the detector would be

$$V_o = \Re\Phi = 69 \times 4.0 \times 10^{-19}\left(T_a^4 - T_d^4\right) \tag{6–66}$$

If we use the source temperature as 650 K, then

$$V_o = \Re\Phi = 69 \times 4.0 \times 10^{-19}\left(650^4 - 0^4\right) = 4.9\mu V \tag{6–67}$$

For the non cooled case, where the detector, detector housing and radiometer tube are all at room temperature, $T = 296$ K

$$V_o = \Re\Phi = 69 \times 4.0 \times 10^{-19}\left(650^4 - 296^4\right) = 4.7\mu V \tag{6–68}$$

An ideal cooler would only increase the signal by 0.2 μV, which is 4 percent. Detector cooling is beneficial for a system where the configuration factor is large but the source is weak. Cooling then greatly increases the $\left(T_a^4 - T_d^4\right)$ term, which increases the output. For this radiometer the small configuration factor, i.e. small FOV and small aperture, is the cause of the low signal level. Cooling the detector will not significantly increase the radiometer output, and if not tightly regulated may introduce additional errors due to temperature differences between the detector and the radiometer tube. For these reasons detector cooling is not used for this design.

7. Radiometer Design

The design of a lensless radiometer involves determining the proper detector size, aperture size and spacing between the detector and aperture in order to obtain the desired FOV and working distance. For the FEANICS/ REEFS experiment the following parameters are fixed

Top Radiometer
Pinhole to fuel surface working distance, S_{do} = 120 mm
Maximum detector to pinhole spacing, S_{da} = 30 mm
FOV = 2.5 mm

Bottom Radiometer
Pinhole to fuel surface working distance, S_{do} = 12 mm
Maximum radiometer length (including housing and wiring), S_{da} = 12.65 mm
FOV = 2.5 mm

Once the above fixed parameters are known, the next step in designing the radiometer is to determine the detector and aperture size. According to equations (3–5) and (3–6), the diameter of the umbra and penumbra will be

$$D_u = \frac{D_a\left(S_{da} + S_{ao}\right) - D_d S_{ao}}{S_{da}} \text{ (umbra)} \tag{7–1}$$

$$D_p = \frac{D_a\left(S_{da} + S_{ao}\right) + D_d S_{ao}}{S_{da}} \text{ (penumbra)} \tag{7–2}$$

By inspection of these equations, for a fixed S_{da}, S_{ao}, and D_p, it is apparent that a smaller detector diameter will result in less difference between the umbra and penumbra diameter (i.e., $D_p - D_u$ = minimum), which will result in a more well defined FOV. Conversely a smaller detector has a smaller area and a lower throughput, therefore will have a lower output.

There are two models of thermopile detectors under consideration which will arbitrarily be labeled "model A" and "model B". Model A has an active area of 0.25 by 0.25 mm and a responsivity = 193.9 V/W. Model B has an active area of 0.6 by 0.6 mm and a responsivity = 101.0 V/W. Both detectors come in a TO-5 package. The TO-5 package is 8.25 mm in diameter, 8.6 mm tall and the detector to the top of the can spacing is 4.75 mm. The responsivity given on the spec sheet is for the detector with a KBr window and argon encapsulating gas. Since it is desirable to have a circular detector, a circular aperture will be placed directly on the detector. The aperture diameter will be the same dimension as the side for each detector. The thermopile detector responsivity is measured using a calibrated black body simulator with a given aperture, placed at a given distance from the detector. From this the irradiance (H) in watts/cm^2 impinging on the detector can be computed. By measuring the detector output voltage the responsivity can be computed as

$$\Re = \frac{V_s}{HA_d} \quad \left(\frac{V}{W}\right) \tag{7–3}$$

where

A_d the detector area

The aperture placed in front of the detector will reduce the output voltage in proportion to the reduction in detector area, which will be

$$\frac{V_{s2}}{V_{s1}} = \frac{A_2}{A_1} = \frac{\left(\frac{\pi D^2}{4}\right)}{D^2} = \frac{\pi}{4} \tag{7–4}$$

In order to accommodate the desired spectral range the detector window will be KRS-5 which has a transmission, $\tau = 0.72$. The transmission of KBr is, $\tau = 0.92$. This will further reduce the output voltage by a factor of

$$\frac{V_2}{V_1} = \frac{\tau_2}{\tau_1} = \frac{0.72}{0.92} = 0.78 \tag{7–5}$$

The encapsulating gas directly affects the output voltage and time response of the radiometer. Since an extremely low signal is expected for these radiometers Xenon is chosen as the encapsulating gas. For the detectors under consideration Xenon gas will increase the output voltage by a factor of 1.6 vs. argon gas.

$$\frac{V_2}{V_1} = 1.6 \tag{7–6}$$

Taking into account equations (7–4), (7–5), and (7–6), the thermopile detector manufacturer's calibration test conditions with the corresponding output voltage provided on the calibration sheets (V_s = 40 for model A, V_s = 120 for model B) and the detector configuration described above the expected output voltage for each detector will be

$$V_A = V_s\left(\frac{A_2}{A_1}\right)\left(\frac{\tau_2}{\tau_1}\right)(1.6) = 40\left(\frac{\pi}{4}\right)\left(\frac{0.72}{0.92}\right)(1.6) = 39.4 \quad \left(\frac{V}{W}\right) \tag{7–7}$$

$$V_B = V_s\left(\frac{A_2}{A_1}\right)\left(\frac{\tau_2}{\tau_1}\right)(1.6) = 120\left(\frac{\pi}{4}\right)\left(\frac{0.72}{0.92}\right)(1.6) = 118 \quad \left(\frac{V}{W}\right) \tag{7–8}$$

The expected responsivity for each detector using the manufacturer's calibration test conditions and the detector configuration described above will be

$$\frac{\Re_2}{\Re_1} = \frac{\left(\frac{V_{s2}}{HA_{d2}}\right)}{\left(\frac{V_{s1}}{HA_{d1}}\right)} = \frac{\tau_2}{\tau_1}(1.6) \tag{7–9}$$

$$\Re_A = 193.9\left(\frac{0.72}{0.92}\right)(1.6) = 242.8 \quad \left(\frac{V}{W}\right) \tag{7–10}$$

$$\Re_B = 101.0\left(\frac{0.72}{0.92}\right)(1.6) = 126.5 \quad \left(\frac{V}{W}\right) \tag{7–11}$$

It is interesting to note that the reduction in detector area does not affect the responsivity of the detector. The responsivity is a measure of detector output voltage vs. input power, if the detector area is reduced both of these quantities will be reduced proportionally and the responsivity will remain constant.

In theory these detectors appear to have a fairly high responsivity even with the apertures on top of the detectors. Unfortunately, in practice these responsivities are not obtainable with the chosen thermopile detectors and the arrangement described above. The active area of the detector is supported by a membrane inside of the detector housing which has a surface area larger than the detector active area. Although theoretically there should not be any heat transfer from the membrane, in practice this is not true. This results in the actual detector area being equal to the membrane area instead of the active area. In addition the responsivity is not uniform over the entire area, it is higher on the active area than on the membrane. Because of this we cannot simply use the provided calibration sheets and calculate the responsivity based on the changes from the calibration conditions. The responsivity must be measured for our specific configuration. The importance of using a well defined aperture on the detector active area should also be noted. If an aperture is not placed on the active area and the active area dimension is used to compute the field of view, then obviously the calculations will be incorrect. In addition since the detector active area will be surrounded by a less sensitive membrane area, the umbra/penumbra effect will be increased.

Typical test data provided by the manufacturer for the model B detector, with a 0.6 mm aperture on top of the active area, KRS-5 window and Xenon back fill gas, gives an output voltage = 66 μV. The test conditions are, black body temperature T_{bb} = 500 K, room temperature T_r = 296 K, black body aperture A_t = 0.6513 cm at a distance d = 10 cm. These conditions give H = 330 μW/cm^2. From this we can calculate a typical responsivity for the model B detector as

$$\Re_B = \frac{V_s}{HA} = \frac{66}{330\left(\frac{\pi}{4}(0.06)^2\right)} = 71 \quad \left(\frac{V}{W}\right) \tag{7–12}$$

Unfortunately no test data was obtained for the model A detectors so the responsivity was measured in the lab. The test conditions were black body temperature T_{bb} = 552 K, room temperature T_r = 296 K, black body aperture A_t = 0.6513 cm at a distance d = 10 cm. The irradiance can be calculated as

$$H = \frac{\sigma A_t}{\pi d^2}\left(T_{bb}^4 - T_r^4\right) = 512 \quad \left(\frac{\mu W}{cm^2}\right) \tag{7–13}$$

The test was conducted for both a model A detector and a model B detector. The measured voltage for each detector was

$$V_B = 100\mu V$$

$$V_A = 10.8\mu V$$

The responsivity for each detector is

$$\Re_B = \frac{V_B}{HA_B} = \frac{100}{512\left(\frac{\pi}{4}(0.06)^2\right)} = 69 \quad \left(\frac{V}{W}\right) \tag{7–14}$$

$$\Re_A = \frac{V_A}{HA_A} = \frac{10.8}{512\left(\frac{\pi}{4}(0.025)^2\right)} = 43 \quad \left(\frac{V}{W}\right) \tag{7–15}$$

The measured responsivity for the model B detector agrees reasonably well with the data provided by the manufacturer, $\Re_B = 71 \quad (V/W)$ (Eq. (7–12)).

Data provided by the Principal Investigator from REEFS tests in the NASA Glenn Research Center 2.2 second drop tower using the radiometer shown in figure 4 yields detector irradiance on the order of E = 1500 to 3000 μW/cm^2. The detector used was a miniature thermopile detector with a 0.55 by 0.51 mm actual detector size and a CaF window, τ = 0.9. The radiometer had an aperture diameter = 2 mm spaced 3.75 mm from the detector. For E = 3000 μW/cm^2 the total net radiant power on the detector is

$$\Phi = EA_d = (3000)(0.051)(0.055) = 8.42\ \mu W \tag{7–16}$$

Using equations (4–5) and (4–6), the radiance of the source, L, with respect to the detector is

$$L = \frac{\Phi}{throughput} = \frac{\Phi}{\left(\frac{\tau A_t A_d}{d^2}\right)} = \frac{8.42\times10^{-6}}{\left(\frac{(0.9)(0.051)(0.055)(0.2)^2\left(\frac{\pi}{4}\right)}{3.75^2}\right)} = 1.49 \quad \left(\frac{W}{cm^2 sr}\right) \tag{7–17}$$

The exitance of the source, M, with respect to the detector is

$$\Delta M = \pi L = 4.69 \quad \left(\frac{W}{cm^2}\right) \tag{7–18}$$

From the Stefan-Boltzmann law, equation (6–30)

$$\Delta M = \sigma\left(T^4 - T_d^4\right) \tag{7–19}$$

where detector temperature = $T_d = 296K$
T equivalent black body temperature of the source.
T = 956 K

This test was for a relatively strong flame that would not be tested in space. The flames in space are expected to be on the order of 1/3 of what was tested in the drop tower. Using the same radiometer configuration shown in figure 4 these flames would yield a detector irradiance on the order of E = 500 to 1000 μW/cm^2. Following the above example these irradiances give an equivalent black body temperature of the source T = 659 K and 766 K for E = 500 and 1000 μW/cm^2, respectively.

Table 4 was used to determine the optimal detector and aperture size combination for the REEFS top radiometer. The 2.2 second drop tower radiometer shown in figure 4 is also listed in this table for comparison. As can be seen in table 4 the radiometer output will be significantly lower than the output obtained in the 2.2 second drop tower tests. For the penumbra at the fuel surface to be less than the desired 2.5 mm the radiometer output will be less than 1 μV, which is not practical. Configuration #15 utilizing the model B detector and a 0.3 mm pinhole aperture was chosen as a compromise between small FOV and large output voltage. The penumbra of this configuration is 3.9 mm at the fuel surface. Given that the radiometer is more sensitive in the center of its FOV due to the umbra-penumbra phenomena, and since meaningful data was obtained in the 2.2 second drop tower testing with a much larger FOV, the Principal Investigator determined that the FOV extending past the diameter of the hole in the fuel was acceptable. This configuration is expected to have an output signal of approximately 5 μV.

Table 5 shows the comparison for the REEFS bottom radiometer. The pinhole sizes listed in the table are standard pinhole sizes available from the manufacturer. Configuration #7 was chosen, utilizing the model B detector and a 0.61 mm pinhole aperture. This configuration yields a 2.32 mm penumbra, a 0.62 mm umbra and an expected output voltage of 257 μV, which is significantly higher than the top radiometer output.

For tables 4 and 5, values in black are entered data while values in color are calculated. The calculated values were obtained using the following formulas.

Umbra—equation (3–5)

$$D_u = \frac{D_a\left(S_{da} + S_{ao}\right) - D_d S_{ao}}{S_{da}} \tag{7–20}$$

Penumbra—equation (3–6)

$$D_p = \frac{D_a\left(S_{da} + S_{ao}\right) + D_d S_{ao}}{S_{da}} \tag{7–21}$$

Throughput **(Φ_{det}/L_s)**—equation (4–5) ($\tau = 1$ since it is included in the responsivity)

$$Throughput = \frac{\tau A_d A_a}{S_{da}^2} \tag{7–22}$$

Output Voltage/L_s **(V_o/L)**—equations (4–3), (4–5), and (5–13)

$$\Phi = \left(Throughput\right)L \quad (4–3) \tag{7–23}$$

$$Throughput = \frac{\tau A_d A_a}{S_{da}^2} \quad (4–5) \tag{7–24}$$

$$\Re = \frac{V_o}{\Phi} \quad (5–13) \tag{7–25}$$

Rearranging equation (5–13) and substituting equation (4–3)

$$V_o = \Re\Phi = \Re\left(Throughput\right)L \tag{7–26}$$

Rearranging equation (7–26) and substituting equation (4–5) with $\tau = 1$

$$\frac{V_o}{L} = \Re\left(Throughput\right) = \frac{\Re A_d A_a}{S_{da}^2} \tag{7–27}$$

Radiometer Output Voltage (V_o)—equations (5–11), (5–12), and (5–13)

$$\Phi = \frac{\tau A_d A_a \left(L_s - L_d\right)}{S_{da}^2} \quad (5\text{–}11) \tag{7–28}$$

$$L = \frac{\varepsilon \sigma T^4}{\pi} \quad (5\text{–}12) \tag{7–29}$$

$$\Re = \frac{V_o}{\Phi} \quad (5\text{–}13) \tag{7–30}$$

Rearranging equation (5–13)

$$V_o = \Re \Phi \tag{7–31}$$

Substituting equation (5–12) into equation (5–11)

$$\Phi = \frac{\tau A_d A_a \varepsilon \sigma \left(T_s^4 - T_d^4\right)}{\pi S_{da}^2} \tag{7–32}$$

Substituting equation (7–32) into equation (7–31) and set $\tau = 1$, $\varepsilon = 1$

$$\boxed{V_o = \frac{\Re A_d A_a \sigma \left(T_s^4 - T_d^4\right)}{\pi S_{da}^2} = \frac{V_o}{L} \frac{\sigma}{\pi} \left(T_s^4 - T_d^4\right)} \tag{7–33}$$

Table 4.—REEFS top radiometer design comparisons

Configuration	Radiometer	Responsivity (V/W)	Detector Diameter (mm)	Pinhole Diameter (mm)	Detector to Pinhole Distance (mm)	Distance from Pinhole to Object Plane (mm)	Umbra (mm)	Penumbra (mm)	Throughput, Φ_{det}/L_s (μW/(W/sr·cm^2)	Output Voltage/L_s (μV/(W/sr·cm^2)	Target Temp (K)	Detector Temp (K)	Radiometer Output Voltage (uV)
2.2 Sec Drop		40	0.6	2.00	37.5	75	4.80	7.20	6.3165	252.66	956.00	296.00	377.39
2.2 Sec Drop		40	0.6	2.00	37.5	75	4.80	7.20	6.3165	252.66	659.00	296.00	82.50
1	Model A	43	0.25	0.25	30	120	0.25	2.25	0.0268	1.15	659.00	296.00	0.38
2	Model A	43	0.25	0.30	30	120	0.50	2.50	0.0386	1.66	659.00	296.00	0.54
3	Model A	43	0.25	0.40	30	120	1.00	3.00	0.0685	2.95	659.00	296.00	0.96
4	Model A	43	0.25	0.50	30	120	1.50	3.50	0.1071	4.60	659.00	296.00	1.50
5	Model A	43	0.25	0.60	30	120	2.00	4.00	0.1542	6.63	659.00	296.00	2.17
6	Model A	43	0.25	0.70	30	120	2.50	4.50	0.2099	9.03	659.00	296.00	2.95
7	Model A	43	0.25	0.80	30	120	3.00	5.00	0.2742	11.79	659.00	296.00	3.85
8	Model A	43	0.25	0.90	30	120	3.50	5.50	0.3470	14.92	659.00	296.00	4.87
9	Model A	43	0.25	1.00	30	120	4.00	6.00	0.4284	18.42	659.00	296.00	6.01
10	Model A	43	0.25	1.10	30	120	4.50	6.50	0.5183	22.29	659.00	296.00	7.28
11	Model A	43	0.25	1.20	30	120	5.00	7.00	0.6169	26.52	659.00	296.00	8.66
12	Model A	43	0.25	1.30	30	120	5.50	7.50	0.7239	31.13	659.00	296.00	10.16
13	Model B	69	0.6	0.10	30	120	-1.90	2.90	0.0247	1.70	659.00	296.00	0.56
14	Model B	69	0.6	0.20	30	120	-1.40	3.40	0.0987	6.81	659.00	296.00	2.22
15	Model B	69	0.6	0.30	30	120	-0.90	3.90	0.2221	15.32	659.00	296.00	5.00
16	Model B	69	0.6	0.40	30	120	-0.40	4.40	0.3948	27.24	659.00	296.00	8.89
17	Model B	69	0.6	0.50	30	120	0.10	4.90	0.6169	42.56	659.00	296.00	13.90
18	Model B	69	0.6	0.60	30	120	0.60	5.40	0.8883	61.29	659.00	296.00	20.01
19	Model B	69	0.6	0.70	30	120	1.10	5.90	1.2090	83.42	659.00	296.00	27.24
20	Model B	69	0.6	0.80	30	120	1.60	6.40	1.5791	108.96	659.00	296.00	35.58
21	Model B	69	0.6	0.90	30	120	2.10	6.90	1.9986	137.90	659.00	296.00	45.03
22	Model B	69	0.6	1.00	30	120	2.60	7.40	2.4674	170.25	659.00	296.00	55.59

Table 5.—REEFS bottom radiometer design comparisons

Configuration	Radiometer	Responsivity (V/W)	Detector Diameter (mm)	Pinhole Diameter (mm)	Detector to Pinhole Distance (mm)	Distance from Pinhole to Object Plane (mm)	Umbra (mm)	Penumbra (mm)	Throughput, Φ_{det}/L_s (μW/(W/sr·cm^2)	Output Voltage/L_s (μV/(W/sr·cm^2)	Target Temp (K)	Detector Temp (K)	Radiometer Output Voltage (uV)
1	Model A	43	0.25	0.61	8.5	12	1.12	1.82	1.9856	85.38	659.00	296.00	27.88
2	Model A	43	0.25	0.75	8.5	12	1.46	2.16	3.0015	129.07	659.00	296.00	42.14
3	Model A	43	0.25	1.00	8.5	12	2.06	2.76	5.3361	229.45	659.00	296.00	74.92
4	Model A	43	0.25	1.25	8.5	12	2.66	3.37	8.3376	358.52	659.00	296.00	117.07
5	Model A	43	0.25	1.50	8.5	12	3.26	3.97	12.0062	516.27	659.00	296.00	168.58
6	Model A	43	0.25	2.00	8.5	12	4.47	5.18	21.3443	917.80	659.00	296.00	299.69
7	Model B	69	0.6	0.61	8.5	12	0.62	2.32	11.4368	789.14	659.00	296.00	257.68
8	Model B	69	0.6	0.75	8.5	12	0.96	2.66	17.2889	1192.93	659.00	296.00	389.53
9	Model B	69	0.6	1.00	8.5	12	1.56	3.26	30.7358	2120.77	659.00	296.00	692.50
10	Model B	69	0.6	1.25	8.5	12	2.17	3.86	48.0247	3313.70	659.00	296.00	1082.04
11	Model B	69	0.6	1.50	8.5	12	2.77	4.46	69.1555	4771.73	659.00	296.00	1558.13
12	Model B	69	0.6	2.00	8.5	12	3.98	5.67	122.9432	8483.08	659.00	296.00	2770.01

8. Baffling

Baffles are additional apertures placed between the detector and the field stop (the FOV limiting front aperture). The purpose of the baffles is to block internal reflections in order to eliminate radiation from outside of the intended FOV from impinging on the detector. As shown in figure 13, for the simple lensless radiometer, radiation from outside of the FOV can enter the radiometer through the field stop, reflect off of the radiometer tube wall and impinge on the detector.

In order to design the baffle system the radiometer geometry must be known. The FEANICS/ REEFS top radiometer configuration, excluding the baffles, is shown in figure 14. The radiometer consists of the thermopile detector and its housing, the field stop aperture and a tube to connect the two pieces. The top radiometer assembly consists of two identical radiometer systems, parallel to each other and spaced 11 mm apart, centerline to centerline. Since each radiometer system is identical, only one will be shown here. A 3-D model of the FEANICS/REEFS top radiometer assembly is shown in figure 20.

The on-axis alignment of the components is another factor that needs to be taken into account for the design of the baffle system. Ideally the detector, baffles and the field stop aperture all should be on the same optical axis. The detector manufacturer states that the detector on axis tolerance is ±0.25 mm. The field stop aperture was designed with an on axis adjustment of ±0.75 mm. The baffles are fixed and mechanically centered in the radiometer tube bore, therefore they are always assumed to be on axis. Since the field stop aperture has an on axis adjustment of ±0.75 mm, the design will also permit a detector on axis tolerance of ±0.75 mm. This increase in the detector on axis tolerance over the manufacturers stated tolerance provides a margin of error for machining and assembly. The field stop adjustment is provided to insure the optical axis connecting the detector and the field stop remains parallel to the radiometer tube bore. The baffle system must be designed for the worst case scenario which is when the detector and the field stop are off axis by 0.75 mm.

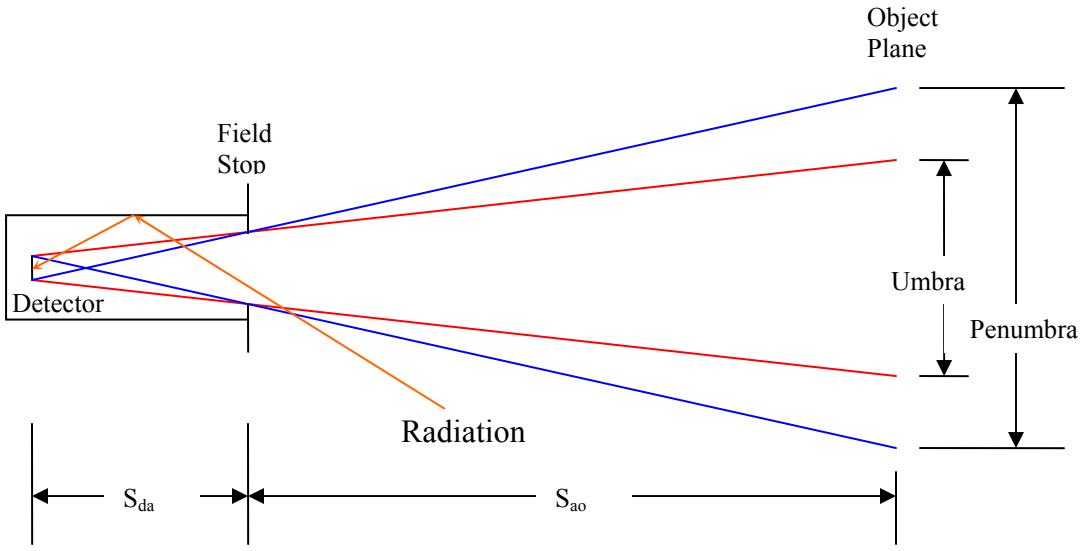

Figure 13.—Radiation outside of FOV impinging on detector.

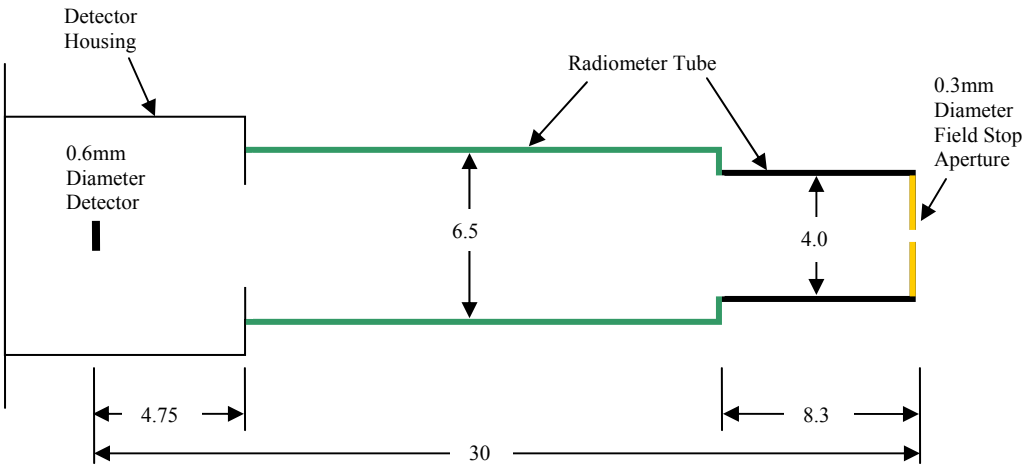

All Dimensions in mm

Figure 14.—FEANICS/REEFS top radiometer, excluding baffles.

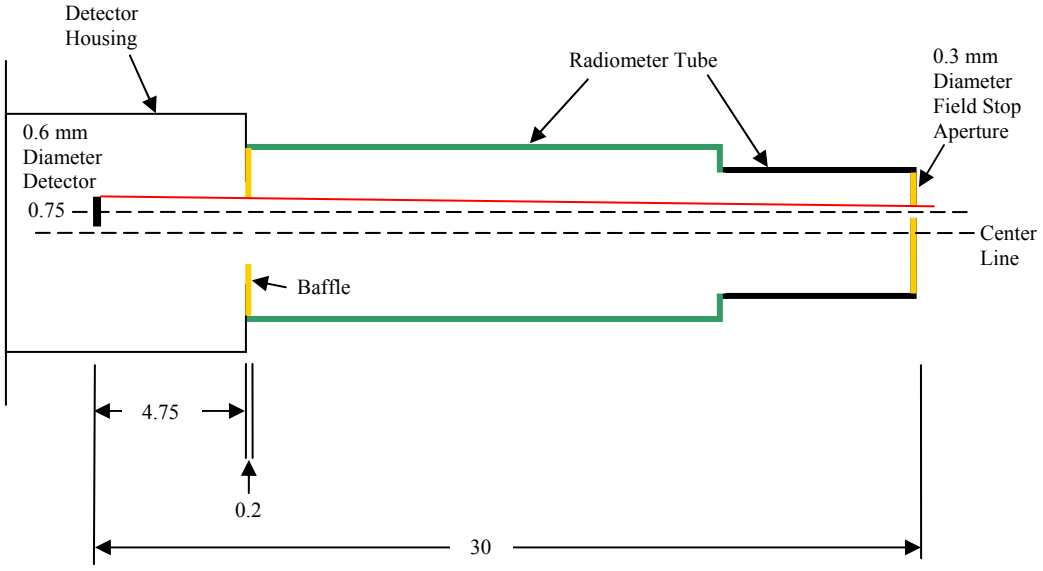

All Dimensions in mm

Figure 15.—Determination of top radiometer baffle diameter.

The baffles will be stock pinholes 0.2 mm thick. The standard pinhole sizes are; 2.0, 1.5, 1.25, 1.0, 0.75, and 0.61 mm. Since the radiometer in this application is so temperature sensitive, the first baffle will be placed as close to the detector as possible. Placing the baffle close to the detector will help insure that the baffle temperature is the same as the detector temperature. For this reason the first baffle location will be used as the starting point of the design.

The first step in the baffle design is to determine the baffle opening diameter to insure that the desired signal through the field stop is not attenuated. Figure 15 shows the radiometer with the first baffle in place. The baffle diameter can be determined by calculating the point at which the line connecting the top of the detector and the top of the field stop intersects the baffle.

An exploded view of the geometry is shown in figure 16.

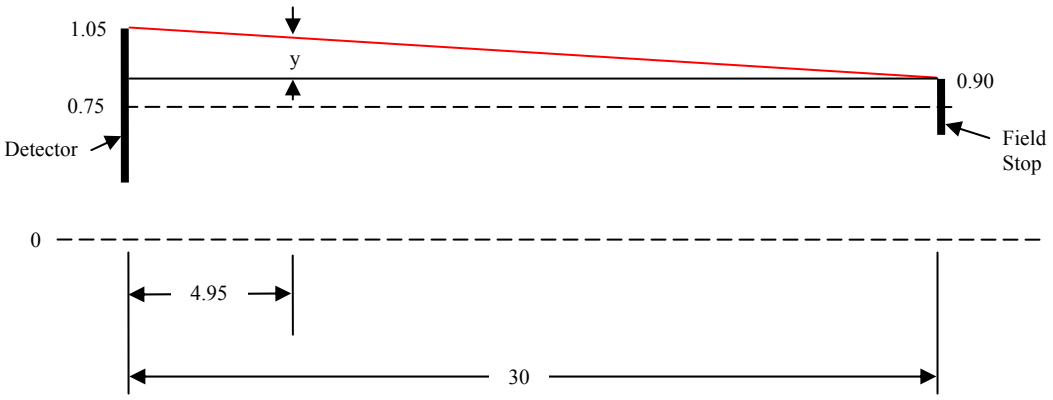

All Dimensions in mm

Figure 16.—Geometry to calculate top radiometer baffle diameter.

From similar triangles

$$\frac{(1.05 - 0.90)}{30} = \frac{y}{(30 - 4.95)} \tag{8–1}$$

$$y = 0.125 \text{ mm} \tag{8–2}$$

$$\textit{Baffle Diameter} = 2(0.9 + y) = 2.05 \text{ mm} \tag{8–3}$$

The standard 2.0 mm baffle will be used since the 0.75 mm adjustment is more than ample given the detector manufacturer specification of on axis ±0.25 mm.

The next step is to determine the point up to which the 2.0 mm baffle will block the tube wall reflections.

Referring to figure 17, the 2.0 mm baffle will block all radiometer tube wall reflections from the baffle location to location x. An exploded view of the geometry is shown in figure 18.

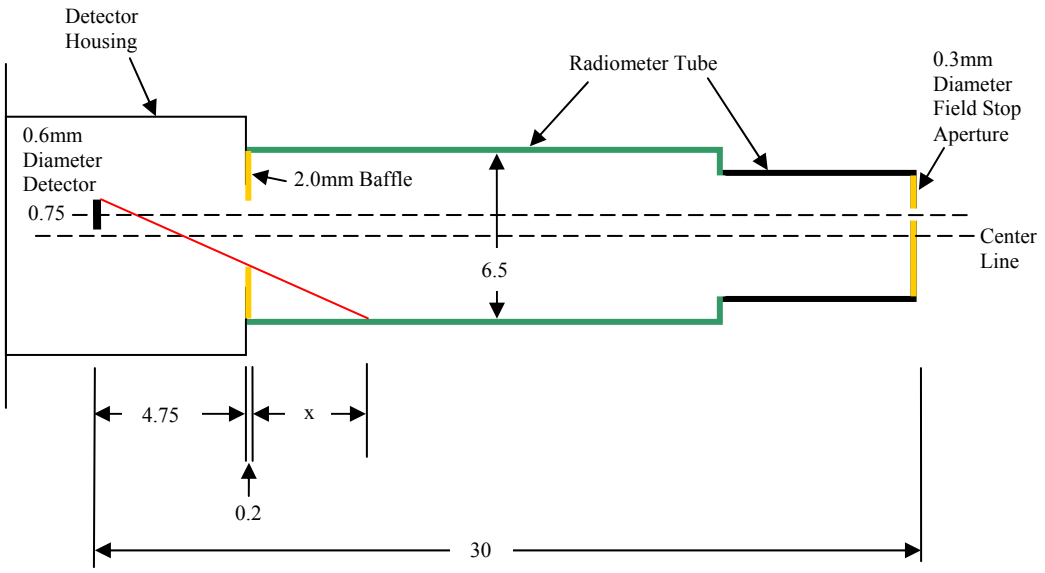

All Dimensions in mm

Figure 17.—Determination of top radiometer baffle coverage.

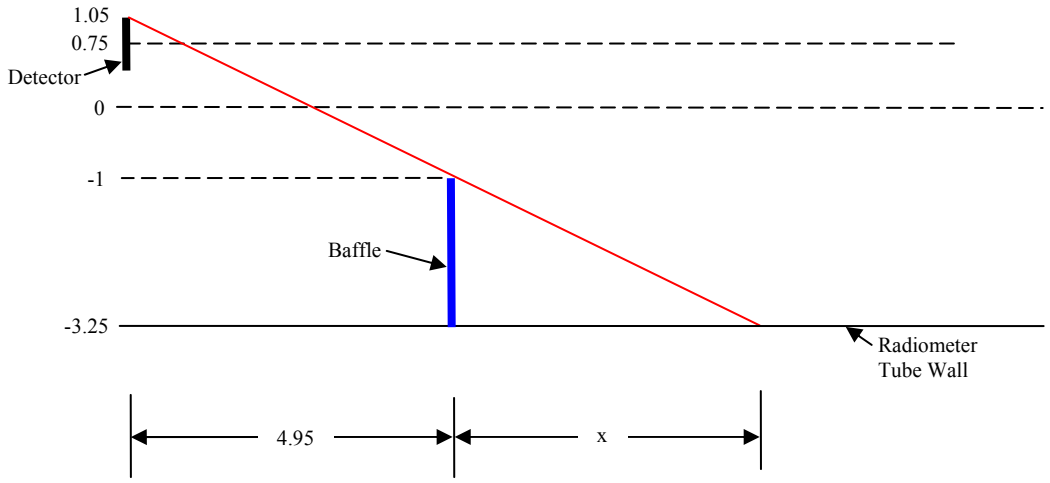

All Dimensions in mm

Figure 18.—Geometry to calculate top radiometer baffle coverage.

From similar triangles

$$\frac{x}{(3.25-1)} = \frac{(4.95+x)}{(3.25+1.05)} \tag{8–4}$$

$$\frac{x}{2.25} = \frac{(4.95+x)}{4.30} \tag{8–5}$$

$$4.30x = 2.25(4.95) + 2.25x \tag{8–6}$$

$$x(4.30-2.25) = 11.14 \tag{8–7}$$

$$x = 5.4 \text{ mm} \tag{8–8}$$

The first baffle will block all reflections emanating from the tube wall out to 5.4 mm from the baffle surface. Since this does not extend out to the field stop another baffle needs to be placed at 5.4 mm from the first baffle.

The same procedure outlined above for the first baffle calculations is used for all subsequent baffles. The baffle diameter is chosen as the closest standard size aperture that is greater than or equal to the calculated size. The process ends when a baffle will block all tube reflections to a point past the field stop, which is greater than 30 mm from the detector.

The final top radiometer design including baffles is shown in figure 19. A 3-D model of the top radiometer assembly is shown in figure 20.

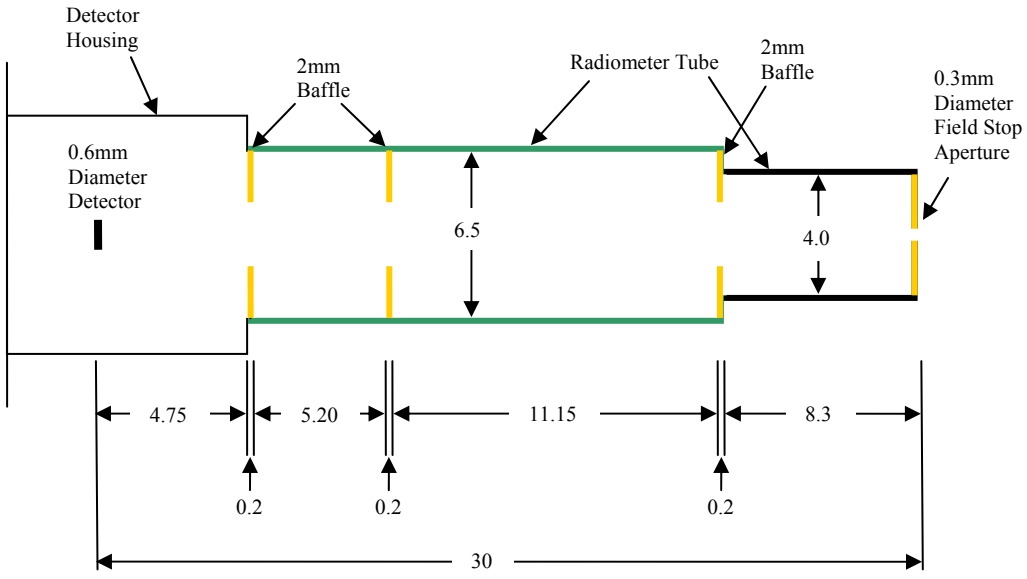

All Dimensions in mm

Figure 19.—REEFS top radiometer final design.

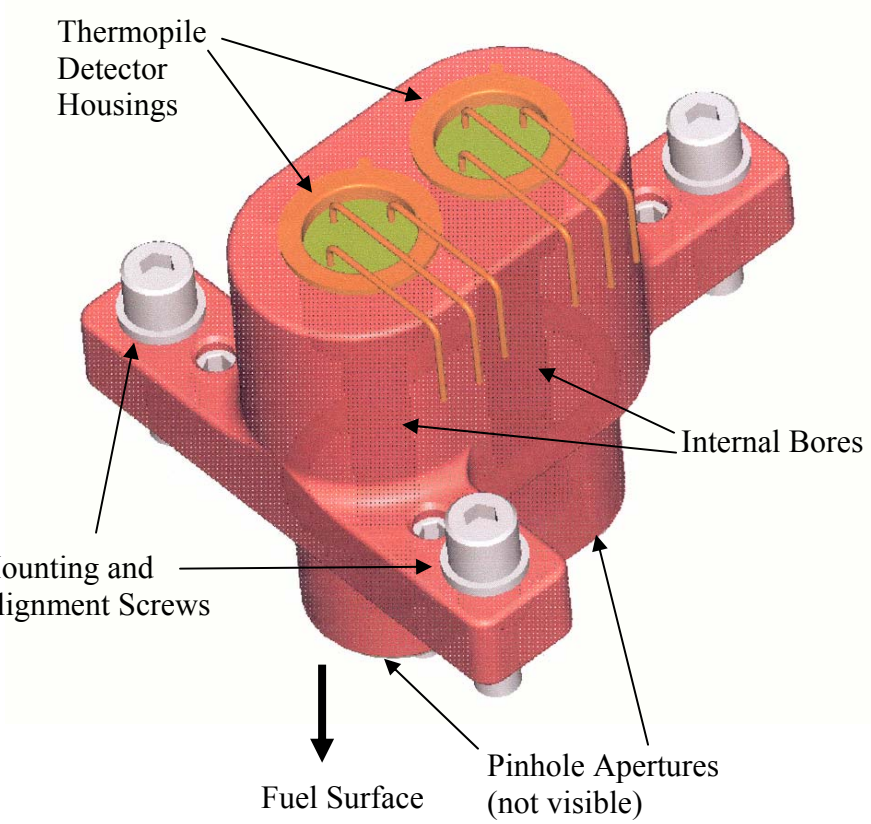

Figure 20.—REEFS top radiometer.

The REEFS bottom radiometers will be as shown in figure 21.

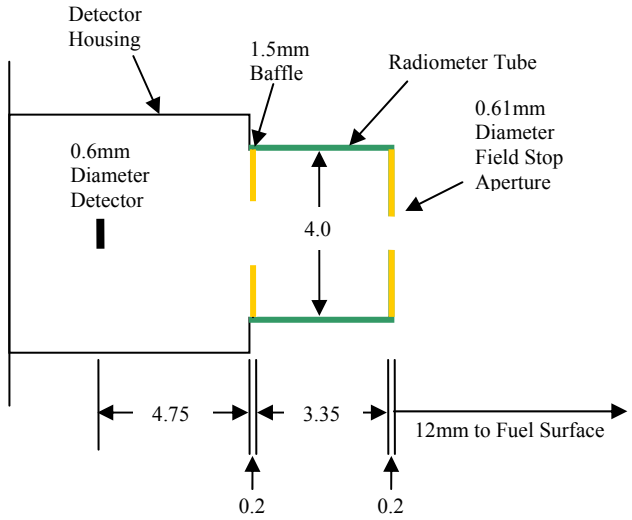

All Dimensions in mm

Figure 21.—REEFS bottom radiometer final design.

The detector to field stop distance and the field stop to fuel surface distance for the bottom radiometer are determined by the REEFS sample boat geometry and space constraints. There is not a field stop aperture adjustment on the bottom radiometer, the off axis allowance is the detector manufacturer specification of on axis ± 0.25 mm. The field stop is assumed to have the same ± 0.25 mm on axis tolerance. The baffle is placed on top of the detector housing and its diameter is calculated assuming worst case, the detector and field stop are 0.25 mm off axis. An exploded view of this geometry is shown in figure 22.

Since the detector and field stop are essentially the same diameter, the minimum baffle diameter is the field stop diameter plus the offset. Referring to figure 22 the bottom radiometer minimum baffle diameter = 2(0.555) = 1.11 mm. The 1.5 mm aperture was chosen for the baffle to give extra allowance for off axis misalignment. Figure 23 shows an exploded view of the geometry with the baffle in place.

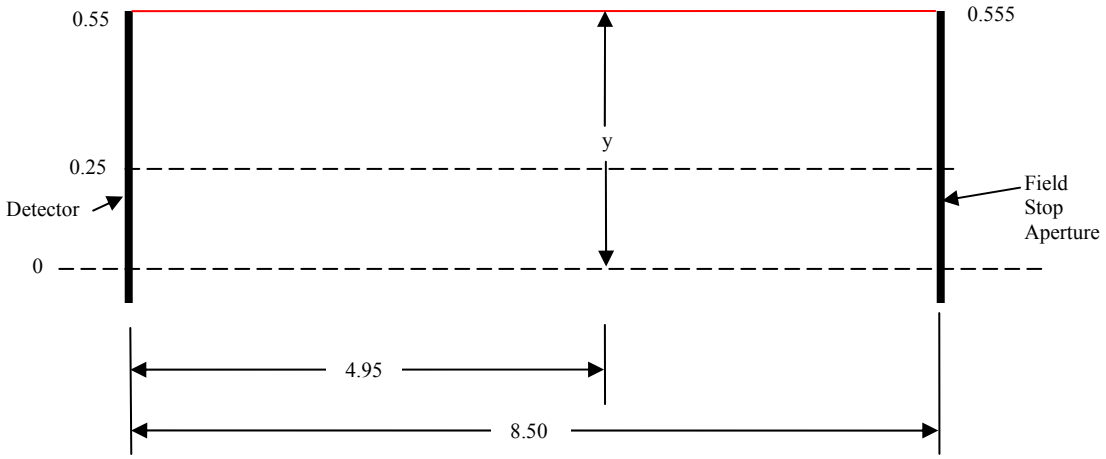

Figure 22.—Geometry to calculate bottom radiometer baffle diameter.

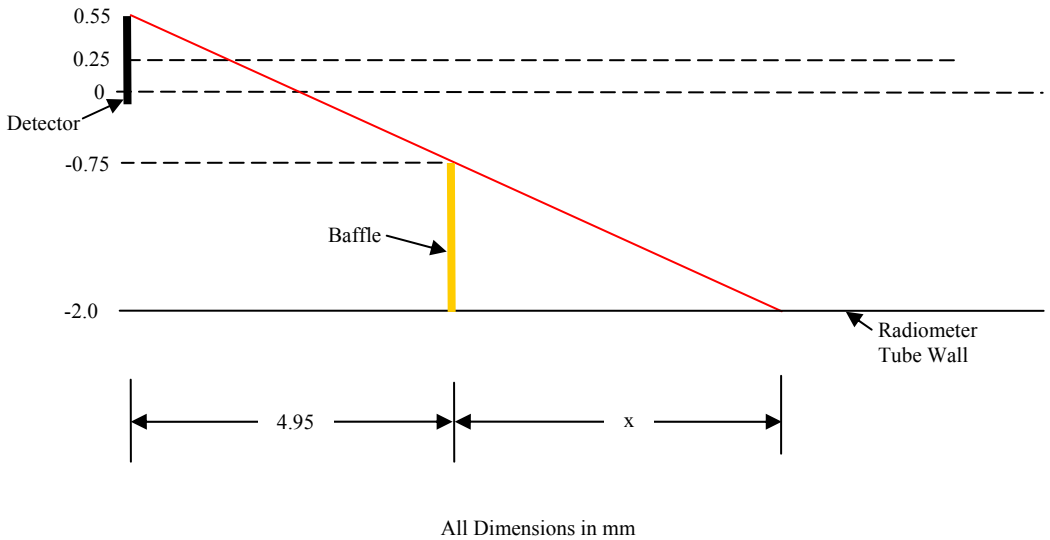

Figure 23.—Geometry to calculate bottom radiometer baffle coverage.

The distance to which the baffle will block all tube wall reflections can be calculated using similar triangles.

$$\frac{x}{(2.0-0.75)} = \frac{(4.95+x)}{(2.0+0.55)} \tag{8–9}$$

$$\frac{x}{1.25} = \frac{(4.95+x)}{2.55} \tag{8–10}$$

$$2.55x = 1.25(4.95) + 1.25x \tag{8–11}$$

$$x(2.55-1.25) = 6.19 \tag{8–12}$$

$$x = 4.76 \text{ mm} \tag{8–13}$$

4.76 mm from the baffle is past the field stop therefore only one baffle is required for the bottom radiometer and the final design will be as shown in figure 21.

9. Amplifiers and Noise

Due to the extremely low expected output from the top radiometers of 5 μV, custom amplifier circuits were designed to amplify these signals for data acquisition. The amplifier circuits are based on an auto-zero chopper stabilized amplifier. This amplifier was chosen to prevent drift which was a major problem with other amplifier designs. The typical drift spec of the auto-zero chopper stabilized amplifier is 0.002 μV/°C. The detector amplifier circuits have two gain sections, a four pole active low pass filter, and conditioning circuitry for temperature sensors. Each thermopile detector has a temperature sensor mounted to the rear of the detector near the thermopile cold junction. The temperature signal is conditioned on the amplifier board to provide a linear 100mv/°C output to the data acquisition system. In order to reduce EMI noise on the radiometer signal an auxiliary circuit board containing the first stage amplifier with gain = 1000, was designed to be locally mounted directly on the rear of the thermopile detector. Figure 24 shows a thermopile detector with the first stage amplifier and temperature sensor.

Referring to equation (6–2), the noise of the voltage of the thermopile detector, V_n, is equal to

$$V_n = \sqrt{4kTRB} \quad Vrms \tag{9–1}$$

where

k Boltzmann's constant, 1.38065×10^{-23} J/K
T detector temperature in Kelvin
R detector resistance in ohms
B detector equivalent noise bandwidth

The equivalent noise bandwidth (ENB) for a four pole low pass filter is

$$ENB = 1.025F_{3dB} = \frac{1.025}{2\pi\tau} = \frac{0.163}{\tau} \quad \text{Hz (ref. 7, p. 453)} \tag{9–2}$$

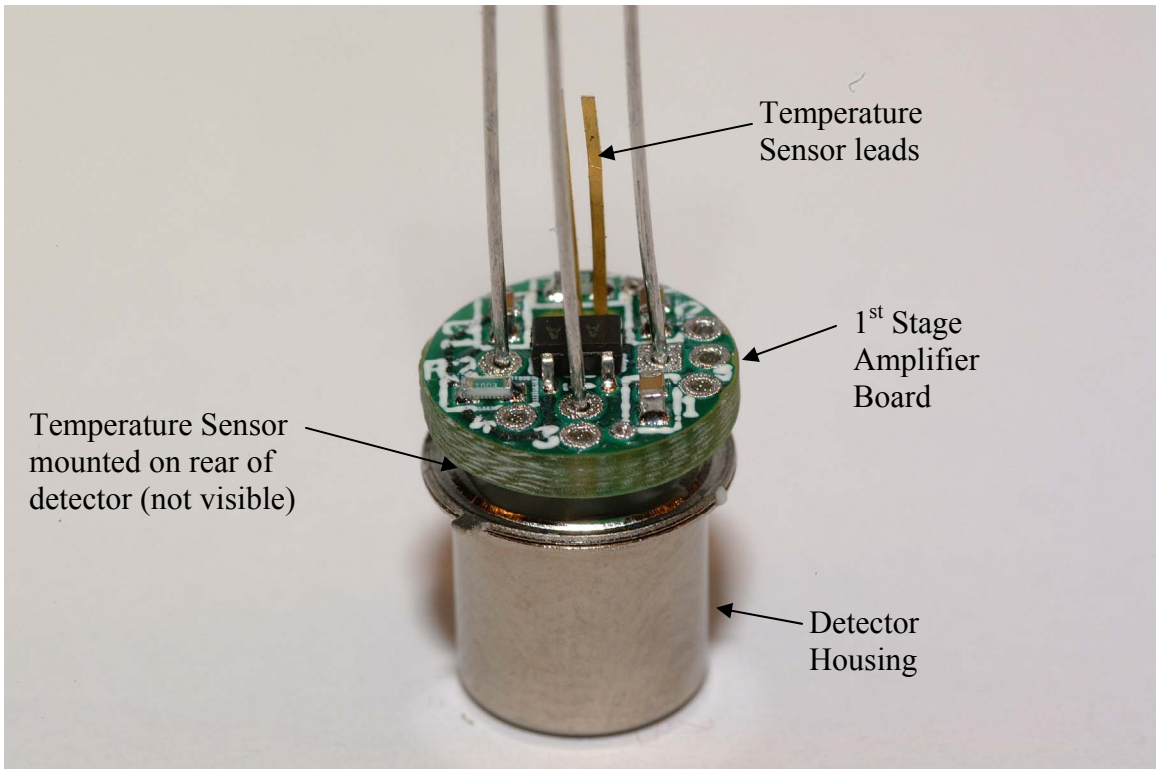

Figure 24.—Thermopile detector and first stage amplifier.

The auto-zero amplifier has a specified input noise voltage = 0.5 μV p-p.

Table 6 summarizes the noise and its effect on the signal to noise ratio (SNR) for the expected signal for both the top and bottom radiometer configurations.

$$SNR = 10\log_{10}\left(\frac{V_s^2}{V_n^2}\right) \quad dB \text{ (ref. 7, p. 434)} \tag{9–3}$$

As can be seen from table 6 the amplifier noise voltage is much larger than the detector noise. The bottom radiometer design has a relatively large SNR. The SNR for the top radiometer is marginal, with the expected full scale signal equal to 10 times the noise signal. Figure 25 shows the results from REEFS test B25-70 conducted in the NASA Glenn Research Center Zero-G facility. This facility is a drop tower capable of providing 5.2 seconds of microgravity. The top radiometer configuration was as described in this report with amplifier gain = 115,845. The bottom radiometer had a slightly different geometry vs. what was described in this report due to differences in the drop rig hardware. The bottom radiometer amplifier gain = 4,177. The three radiometer signals are scaled relative to each other but no specific value of exitance is assigned. The conditions for the test were 35 percent O_2, 65 percent CO_2 at 2 atmosphere pressure.

Table 6.—REEFS radiometer calculated signal and noise voltages

Radiometer	Resp (V/W)	Time Const (mS)	Res (Kohm)	Detector Diameter (mm)	Pinhole Diameter (mm)	Detector to Pinhole Distance (mm)	Distance from Pinhole to Object Plane	Umbra	Pen-umbra
Top - Model B	69	19.2	90	0.6	0.3	30	120	-0.90	3.90
Bottom - Model B	69	19.2	90	0.6	0.61	8.5	12	0.62	2.32

Radiometer	Throughput Φ_{det}/L_s (μW/ (W/sr·cm^2)	Output Voltage/L_s (μV/ (W/sr·cm^2)	Target Temp (K)	Detector Temp (K)	Rad Output Voltage (μV)	Rad Noise Voltage Density (nV/Hz^1/2)	ENB 4section (Hz)	Rad Noise Voltage (nV)	Rad SNR (dB)	Amp Noise Voltage (μV p-p)	Amp SNR (db)	Total SNR (dB)
Top	0.2221	15.32	659.00	296.00	5.00	38.36	8.49	111.76	33.0	0.5	20.0	19.8
Bottom	11.4368	789.14	659.00	296.00	257.68	38.36	8.49	111.76	67.3	0.5	54.2	54.0

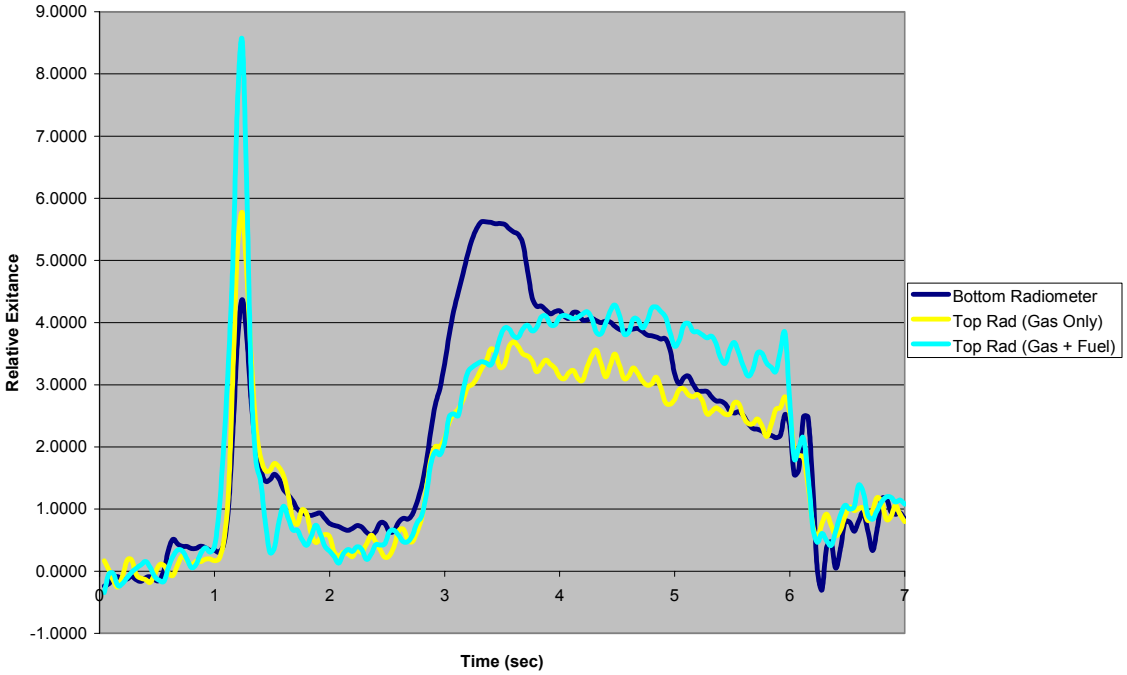

Figure 25.—REEFS radiometer results, test B25-70, NASA GRC Zero-G facility.

The raw data from this test indicates a change in the top radiometer (gas + fuel) = 0.65 V. Dividing this by the gain = 115,845 gives a detector signal V = 5.6 μV, which is very close to the calculated value of 5 μV. The noise voltage ripple on the top radiometer signals measures approximately 0.08V p-p, maximum. Dividing by the gain gives a noise voltage = 0.69 μV p-p at the input of the first amplifier, which is again close to the expected value of 0.5 μV p-p.

10. Conclusion

This report describes the process used to design the FEANICS/REEFS radiometers. Although not included in this report, many ground based experiments were conducted that verify the equations and theories presented. Particular attention needs to be given to temperature effects of the radiometer. As shown in this report and demonstrated via ground testing, these radiometers are extremely sensitive to temperature variations. The radiometer is 37,500 times more sensitive to temperature changes in the detector housing than to temperature changes in the source being measured and 1,700 times more sensitive to temperature changes in the radiometer tube than in the source being measured. The radiometer signal can be easily be lost if proper care is not taken to insure that the radiometer is not subject to temperature variations.

The signal to noise ratio of the top radiometers is marginally acceptable. The expected full scale detector signal is equal to 10 times the amplifier noise signal. Due to the geometric restraints on the working distance and field of view, this is the best that can be done with a lensless design. If the lensed radiometer design was revisited, it can be shown using the equations in section 2 (Design Choices) that a 2.5 mm diameter aperture lens, 30 mm from the detector will blur to 0.32 and 0.34 mm at the extremes of the spectral range. The FOV would expand to 3.84 and 3.93 mm at the extremes of the spectral range (see table 7).

Table 7.—Spectral dependence of blur and FOV, lens diameter = 2.5 mm

Dia Lens (mm)	λ (μm)	n	f (mm)	i (mm)	Δi (mm)	Blur (mm)	FOV (mm)
2.5	1.0	2.45	23.2	28.80	0.00	0.00	2.50
2.5	0.6	2.60	21.0	25.53	3.27	0.32	3.84
2.5	30.0	2.29	26.1	33.37	4.57	0.34	3.93

The throughput of the system would increase by the ratio of the area of the apertures multiplied by the transmission of the lens. For a 2.5 mm, KRS-5 lens the throughput would increase

$$\frac{T_1}{T_2} = \frac{\left(\frac{\pi}{4}\right)(2.5)^2(0.72)}{\left(\frac{\pi}{4}\right)(0.3)^2} = 50 \qquad (10–1)$$

The detector output would be 50 times the current design. This increase in output needs to be weighed against the effect of the focus varying vs. wavelength if a lensed design is to be reconsidered. The availability a KRS-5 lens that meets the radiometer specifications may also be an issue.

Ground based microgravity testing has shown that the lensless radiometer designs described in this report are capable of measuring the radiative flux for the REEFS experiment as specified in the SRD. Temperature sensors and custom amplifiers have been added to the radiometers to help resolve the issues of temperature effects and low signal levels of the radiometers. Breadboard models of these radiometers have proven reliable by providing consistent results in over 50 tests in the NASA Glenn Research Center Zero-G Drop Tower with no apparent degradation. These radiometers, along with their supporting systems, have proven capable of meeting the REEFS science requirements while adhering to the physical and interconnection constraints of the FEANICS hardware.

References

1. E.F. Zalewski. Radiometry and Photmetry, in M. Bass, editor in chief, “Handbook of Optics, Vol II,” 2nd edition, chapter 24. McGraw-Hill, New York, 1995.
2. J.M. Palmer. The Art of Radiometry, draft copy prepared for Optical Sciences 506, University of Arizona, January 2002.
3. J.H. Lienhard IV, J.H. Lienhard V. A Heat Transfer Textbook, 3rd edition, Phlogiston Press, Cambridge, Massachusetts, 2003.
4. R Siegel and J. Howell. Thermal Radiation Heat Transfer, 4th edition, Taylor and Francis, New York, 2002.
5. Application Briefs, in “Thermopile Detectors” Dexter Research Center, Inc., Dexter, Michigan, December 16, 2003.
6. C. DeCusatis, editor. Handbook of Applied Photometry, American Institute of Physics Press, Woodbury, New York, 1997.
7. P. Horowitz and W. Hill. The Art of Electronics, 2nd edition, Cambridge University Press, Cambridge, UK, 1989.

REPORT DOCUMENTATION PAGE

Form Approved
OMB No. 0704-0188

Public reporting burden for this collection of information is estimated to average 1 hour per response, including the time for reviewing instructions, searching existing data sources, gathering and maintaining the data needed, and completing and reviewing the collection of information. Send comments regarding this burden estimate or any other aspect of this collection of information, including suggestions for reducing this burden, to Washington Headquarters Services, Directorate for Information Operations and Reports, 1215 Jefferson Davis Highway, Suite 1204, Arlington, VA 22202-4302, and to the Office of Management and Budget, Paperwork Reduction Project (0704-0188), Washington, DC 20503.

1. AGENCY USE ONLY (*Leave blank*)	2. REPORT DATE	3. REPORT TYPE AND DATES COVERED
	January 2005	Technical Memorandum

4. TITLE AND SUBTITLE

Narrow Angle Wide Spectral Range Radiometer Design
FEANICS/REEFS Radiometer Design Report

5. FUNDING NUMBERS

WBS–22–400–31–30–03

6. AUTHOR(S)

William Camperchioli

7. PERFORMING ORGANIZATION NAME(S) AND ADDRESS(ES)

National Aeronautics and Space Administration
John H. Glenn Research Center at Lewis Field
Cleveland, Ohio 44135–3191

8. PERFORMING ORGANIZATION REPORT NUMBER

E–14947

9. SPONSORING/MONITORING AGENCY NAME(S) AND ADDRESS(ES)

National Aeronautics and Space Administration
Washington, DC 20546–0001

10. SPONSORING/MONITORING AGENCY REPORT NUMBER

NASA TM—2005-213421

11. SUPPLEMENTARY NOTES

Responsible person, William Camperchioli, organization code DDI, 216–433–8301.

12a. DISTRIBUTION/AVAILABILITY STATEMENT

Unclassified - Unlimited
Subject Categories: 35 and 74 Distribution: Nonstandard

Available electronically at http://gltrs.grc.nasa.gov

This publication is available from the NASA Center for AeroSpace Information, 301–621–0390.

12b. DISTRIBUTION CODE

13. ABSTRACT ***(Maximum 200 words)***

A critical measurement for the Radiative Enhancement Effects on Flame Spread (REEFS) microgravity combustion experiment is the net radiative flux emitted from the gasses and from the solid fuel bed. These quantities are measured using a set of narrow angle, wide spectral range radiometers. The radiometers are required to have an angular field of view of 1.2 degrees and measure over the spectral range of 0.6 to 30 μm, which presents a challenging design effort. This report details the design of this radiometer system including field of view, radiometer response, radiometric calculations, temperature effects, error sources, baffling and amplifiers. This report presents some radiometer specific data but does not present any REEFS experiment data.

14. SUBJECT TERMS

Radiometers; Radiance; Temperature effects; Radiative heat transfer

15. NUMBER OF PAGES

52

16. PRICE CODE

17. SECURITY CLASSIFICATION OF REPORT	18. SECURITY CLASSIFICATION OF THIS PAGE	19. SECURITY CLASSIFICATION OF ABSTRACT	20. LIMITATION OF ABSTRACT
Unclassified	Unclassified	Unclassified	